Research Square

Preprints are preliminary reports that have not undergone peer review.
They should not be considered conclusive, used to inform clinical practice,
or referenced by the media as validated information.

PKR Shapes Integrated Stress Response Dynamics to Coordinate Structural and Functional Recovery After Peripheral Nerve Injury

Nicolás W Martínez
Centro Ciencia & Vida
Camila Morales Manzano
Centro Ciencia & Vida
Alejandra Trujillo
Centro Ciencia & Vida
Ignacio S Pizarro
Centro Ciencia & Vida
Daniela Barrera
Centro Ciencia & Vida
Margarita Calvo
Pontificia Universidad Católica de Chile
Soledad Matus
smatus@cienciavida.org

Centro Ciencia & Vida

Research Article

Keywords: PKR (Protein Kinase R), eIF2α phosphorylation, Integrated Stress Response (ISR), Peripheral nerve regeneration, Myelin Basic Protein (MBP), Neurofilament heavy chain (NF-H), Schwann cells, Axonal repair, Motor recovery, Sciatic nerve injury

Posted Date: April 1st, 2026

DOI: https://doi.org/10.21203/rs.3.rs-9204935/v1

License: This work is licensed under a Creative Commons Attribution 4.0 International License.
Read Full License

Additional Declarations: No competing interests reported.

Abstract

Peripheral nerve regeneration requires precise regulation of axonal proteostasis and myelination to restore sensorimotor function after injury. However, whether stress-responsive translational control pathways contribute to this process *in vivo* remains largely unknown. Here, we show that the integrated stress response (ISR), a conserved signaling pathway that fine-tunes the neuronal proteome through kinases that sense intracellular stress, is dynamically activated after sciatic nerve injury and that the RNA-dependent ISR kinase, PKR, shapes the temporal organization of this response during nerve degeneration and regeneration. Peripheral nerve injury triggers a spatially and temporally organized pattern of ISR activation along the injured sciatic nerve. PKR deficiency delays motor recovery after nerve crush without affecting axonal density restoration, while altering ISR activation dynamics and the abundance of nerve integrity markers during degeneration and regeneration. Moreover, loss of PKR impairs the ultrastructural recovery of regenerated nerves, resulting in reduced myelinated axon density and altered g-ratios. Together, these findings identify PKR as a key regulator that couples ISR dynamics to ultrastructural remodeling and functional recovery after peripheral nerve injury.

INTRODUCTION

The peripheral nervous system (PNS) mediates sensory input, motor output, and sensorimotor integration through specialized peripheral nerve circuits [1–7]. These functions depend on the morphological and functional integrity of axons and their associated Schwann cells (SCs) [1–11]. Maintaining the integrity of both unmyelinated and myelinated axons within peripheral nerves requires continuous and spatially restricted regulation of the axonal and glial proteomes through coordinated proteostatic mechanisms, including local protein synthesis and degradation [12–21]. These processes preserve discrete axonal compartments, enable local signal integration, and support the selective maintenance of cytoskeletal and myelin-associated proteins [12, 14, 16, 20, 22–32]. Accordingly, disruption of local proteostatic control impairs axo-glial interactions and progressively compromises nerve function [33–37].

Peripheral nerve integrity is challenged by diverse pathological conditions, including trauma, neurotoxicity, ischemia, inflammation, metabolic disorders, inherited neuropathies such as Charcot–Marie–Tooth disease, and age-related neurodegeneration [34, 38–57]. Despite their distinct etiologies, many of these conditions converge on physical or functional disconnection of distal axons from the neuronal soma [39–41, 55, 58], leading to impaired axonal transport, loss of compartmentalization, and disruption of local proteostasis and axo-glial signaling [36, 37, 59, 60].

Following axonal disconnection, distal axons undergo Wallerian degeneration. This process is initiated by intracellular calcium dysregulation, mitochondrial dysfunction, and oxidative stress, which activate degradative pathways that ultimately lead to loss of axonal compartmentalization, impaired local signaling, and depletion of domain-specific cytoskeletal and myelin proteins [22, 61–71]. Notably,

experimental manipulation of axonal translation can delay degeneration, highlighting translational control as a key determinant of this process [16, 72–74].

Unlike the central nervous system, peripheral nerves retain substantial regenerative capacity [75–77]. After injury, proximal axonal stumps restore membrane integrity, calcium homeostasis, and mitochondrial energy balance [69, 78–91]. Regeneration is highly coordinated and depends on SC reprogramming, extracellular matrix remodeling, and metabolic and trophic support [92–99]. Beyond axonal elongation, successful regeneration requires re-establishment of axonal compartmentalization, selective expression of cytoskeletal and myelin-associated proteins, and restoration of nodal organization [81, 89, 94, 100–105]. Regeneration also depends on the active and precise regulation of local axonal protein synthesis machinery [22, 106], which contributes to proteome remodeling and supports the transition from axonal growth to functional integration between the cellular components of the peripheral nerve [106–108]. Although peripheral nerve regeneration can lead to substantial recovery of sensorimotor function [75, 109–114], remyelination often remains incomplete, with reduced myelin thickness and internodal length limiting full functional restoration [62, 86, 115–117].

The integrated stress response (ISR) is a conserved pathway that couples stress sensing to translational control and adaptive gene expression [118, 119]. ISR activation is mediated by the sensor kinases PKR, PERK, HRI, and GCN2, which sense distinct intracellular perturbations and converge on the phosphorylation of the alpha subunit of eukaryotic initiation factor 2 (eIF2α) [118, 120, 121]. Phosphorylation of eIF2α rapidly suppresses general protein synthesis while increasing the translation of a subset of mRNAs containing upstream open reading frames (uORFs) in their 5’ untranslated regions (UTR) [122–124]. Some of these transcripts subsequently drive adaptive gene expression programs [122–124]. ISR termination occurs via dephosphorylation of eIF2α, restoring translational capacity and allowing cells to adapt or recover, depending on the duration and context of stress [125–127].

Components of the ISR have been implicated in peripheral nerve pathology, largely based on whole-nerve or non-neuronal studies. For example, eIF2α phosphorylation protects Schwann cell function in a murine model of Charcot-Marie-Tooth disease [128]. In Schwann cells, mitochondrial impairment can engage ISR-related programs and contribute to neuropathy [70]. In addition, peripheral nerve injury induces convergent stress signals, including ionic imbalance, mitochondrial dysfunction, oxidative stress, endoplasmic reticulum stress, inflammatory signaling, and metabolic alterations, all of which are known activators of ISR kinases [118, 120, 121]. Notably, the local dynamics of phosphorylated eIF2α control axonal growth in vitro [129].

Despite the reliance of axons on local translation during degeneration and regeneration, and evidence linking proteostasis dysregulation to chronic nerve dysfunction, whether ISR signaling is dynamically engaged in disconnected axonal compartments *in vivo* remains unresolved. Here, we investigated whether ISR signaling links stress sensing to morphological and functional recovery of peripheral nerves after injury. We examined ISR activity during degeneration and regeneration, assessed the contributions of individual eIF2α kinases, and evaluated how modulation of this pathway affects axonal integrity,

myelinated fiber restoration, and motor function recovery. We show that ISR activity is transiently induced after injury and returns to baseline during recovery, and that this temporal regulation is shaped primarily by PKR. Loss of PKR results in defective restoration of myelinated axon architecture and severe motor impairment, indicating that PKR-dependent ISR signaling is required for proper morphofunctional recovery after peripheral nerve injury.

MATERIALS AND METHODS

Animals. Wild-type (WT) C57BL/6 adult male mice were obtained from Jackson Laboratories (Bar Harbor, ME, USA). PKRKO mice (C57BL/6 background) were provided by our collaborator, Dr. Mauro Costa Mattioli. Both WT and PKR-KO mice were housed in groups of four to five per cage in a humidity-controlled environment at 21°C, under a 12-hour light/dark cycle, with ad libitum access to food and water. All animal care and experimental procedures adhered to the guidelines outlined in the Guide for the Care and Use of Laboratory Animals (Commission on Life Sciences, National Research Council, National Academy Press, 1996) and complied with the regulations set by the National Fund for Scientific and Technological Research (FONDECYT-Chile). The experimental protocols, including those involving anesthesia, pain, distress, and euthanasia (No P034/2022, the ethical approval date was May 13, 2022), were approved by the IACUC at the FCV.

Sciatic Nerve Surgery and Post-Operative Timeline. A sciatic nerve crush injury was performed as previously reported. Briefly, an hour before surgery, animals received a subcutaneous injection of ketoprofen (5 mg/kg). Then, 5% isoflurane in air was administered for 3 minutes to induce anesthesia, followed by maintenance at 2% during surgery. For the sciatic nerve injury, the sciatic nerve of the right posterior hindlimb was exposed at the level of the sciatic notch and crushed three times for 5 seconds each with Superfine Dumont #5S forceps. Graphite powder was applied at the crush site and used to identify the nerve segments of interest (3 mm each): (a) the medial segment, which includes the crush site and the downstream adjacent segment, and (b) the distal nerve segment. The left posterior sciatic nerve served as a sham-operated control. Finally, the wound was closed with surgical clips, and animals were returned to their housing until nerve extraction. Nerve segments were collected, or sensorimotor assays were performed at the sham condition or at 3, 7,14, and 21 days post injury (DPI).

Biochemistry. For nerve markers and ISR protein abundance analyses, sciatic nerve segment homogenates were prepared as previously reported [66]. Briefly, sciatic nerves were homogenized at room temperature (RT) using a plastic Dounce in lysis buffer (1% Triton X-100, 50 mM Tris-HCl, pH 6.8, 2 mM EDTA, 1% PMSF, and 1% Protease Inhibitor Cocktail). Then, homogenates were heated for 5 min at 100°C and centrifuged at 13,000 rpm for 10 min at RT. The resulting pellet was resuspended in extraction buffer (5% SDS, 10 mM Tris-HCl, pH 7.4, 2% β-Mercaptoethanol, 1 mM NaF, 1 mM Na_3VO_4, and 1% PIC), heated at 100°C, and centrifuged again at 13,000 rpm for 10 min at RT. The supernatant obtained was stored at -80°C until used for biochemical analysis. Western blot (WB) was performed using SDS-PAGE and polyvinylidene difluoride (PVDF) membranes by standard techniques. Band analysis was performed using ImageJ software (http://rsbweb.nih.gov/ij/). Band intensities were normalized to the total lane

load reported by the Ponceau Red stain. Whole western blot membranes are provided in Supplementary Fig. 7.

Histological Processing for Immunofluorescence and Electron Microscopy. For immunofluorescence (IF) analysis, nerves were fixed by immersion in 4% paraformaldehyde (diluted in 1X PBS, pH 7.4) for 1h, followed by three 10 min washes in 1X PBS, and then dehydrated in an increasing sucrose gradient (5%,10%,20% in 1X PBS) for 1h per percentage. The three washes in 1X PBS were made at each step. Finally, nerves were embedded in OCT, immediately frozen using dry ice, and stored at -80°C. Cryostat sections were cut transversely or longitudinally at 10 µm thickness, mounted on Xylene-coated slides, and stored at -20°C. For IF, mounted sections were washed in 1X PBS for 10 min and then blocked/permeabilized in 0.1% Triton X-100, 2% fish skin gelatin for 1h at RT. Sections were then incubated with primary antibodies in blocking/permeabilizing solution overnight at 4°C, washed three times in 1XPBS for 10 min each, and incubated with secondary antibodies for 2h at RT. Finally, the three PBS 1X washes were repeated, and sections were mounted with Dako Mounting Media and coverslips. For EM analyses, nerve segments were fixed overnight by immersion in 2.5% glutaraldehyde, 0.01% picric acid, and 0.1M cacodylate buffer, pH 7.4. The next day, nerve segments were rinsed in the same buffer and immersed in 1% OsO_4 for 1h, followed by a 2 h block incubation in 2% uranyl acetate. Nerves were dehydrated with a graded series of ethanol, propylene oxide, and infiltrated with Epon. Ultrathin sections were contrasted with 1% uranyl acetate and lead citrate. Grids were examined in a Philips Tecnai 12 electron microscope operated at 80 kV.

Quantification of Axonal Density via IF or EM and g-ratio Calculation. Axonal densities in IFs (axons per 100µm^2) were measured in 20X magnification confocal images of NF-H-immunostained transverse nerve sections (matched for laser power, photomultiplier tube gain/offset, and postprocessing) using the particle analysis macro in FIJI software (http://rsbweb.nih.gov/ij/). Each animal provided a nerve section, resulting in a single image that captured all axonal particles in that section. Three to four animals per group were examined, with five to ten images analyzed per nerve section. Myelinated axonal densities at EM (myelinated axons per 100µm^2) were measured in 1250X magnification TEM images of transverse nerve sections using the Cell Counter macro in FIJI. Each animal contributed one nerve section, and five to ten images per section were analyzed. G-ratios were calculated as the ratio of axon diameter to total fiber diameter, as previously reported. These diameters were obtained from 6000X-magnification TEM images by manually outlining axonal and fiber perimeters using the ROI manager macro in FIJI, then converting these diameters to perimeters using geometric formulas. Each animal contributed one nerve section, and 25 to 30 images per nerve were analyzed.

Sensory Function Assessment by the Von Frey test. Sensory function was assessed by measuring the hind paw withdrawal threshold response to Von Frey filaments. Mice were placed in a transparent box over a mesh floor. Stimulation was performed using the up-and-down method as previously reported [130, 131]. Briefly, Von Frey filaments were applied perpendicular to the mid-plantar area of the anterior crushed hindlimbs, starting with the 5.18 g filament. A positive response was defined as a paw withdrawal or shaking after 2 s touch. After a response, the next lower filament was applied; if there was

no response, the next higher filament was applied. The testing session consists of 5 trials after the first change in response. The response sequence was converted into a 50% withdrawal threshold using the formula: 50% PWT = $10^{(X_f + k\delta)} / 10^4$, where X_f is final von Frey filament used (in log units), k is a value measured from the pattern of positive/negative responses, and $\delta = 0.21$, which is the average interval (in log units) between the von Frey filaments. The mean 50% withdrawal threshold response to touch was determined. Three habituation sessions (30 min each) to the testing area were conducted in three consecutive days, followed by two baseline measurements of hind paw withdrawal threshold on another two consecutive days.

Motor Function Assessment Using the Clasping Test. Motor function was evaluated as the ability to splay the hindlimbs and digits when suspended by the tail (clasping test). In this test, mice were suspended by the base of the tail and recorded for 1 minute. Three separate trials were conducted over three consecutive days as baseline (0 DPI). Hindlimb clasping was scored from 0 to 4 based on the severity of the loss of hindlimb and digit splaying: 0, a clear stereotyped extension of the limb during suspension; complete extension of the fingers; 1, slight deviation from the normal limb position, similar to the control, with slight but noticeable interdigital separation between all digits; 2, abnormal limb position but temporarily normal orientation, with digits 1 and 5 clearly separated and digits 2, 3, and 4 slightly separated; 3, significant impairment of limb motility, with an abnormal angle and no normal positions, slight separation of digits 1 and 5, and digits 2, 3, and 4 remaining together; 4, complete loss of limb motility, inability to move or retraction during suspension, with digits not separated. The overall score was calculated by summing the limb angle score and digital extension score, with a maximum possible motor loss score of 8.

Sciatic Functionality Assessment by Sciatic Functional Index (SFI). Motor function recovery was assessed using the SFI, derived from digital recordings of plantar footprints captured by an infrared-illuminated walkway system, as previously reported [132]. Mice were trained to walk spontaneously along a transparent corridor illuminated from the sides with infrared light, such that paw contact with the surface produced total internal reflection, which was detected by a camera positioned beneath the walkway. The images obtained were processed using a custom automated gait analysis script to extract individual pawprints and measure three parameters for the crushed hindlimbs: print length (PL, distance from the heel to the tip of the third toe), toe spread (TS, distance between the first and fifth toes), and intermediate toe spread (IT, distance between the second and fourth toes). The SFI was calculated using the formula adapted for mice, as previously reported [133]. An SFI value close to 0 indicates normal sciatic nerve function, while values approaching − 100 or lower represent complete functional loss. SFI measurements were obtained at DPI to monitor longitudinal functional recovery.

Statistical Analysis. The normality of data sets was tested using the Shapiro-Wilk test. Based on the results, either parametric or nonparametric tests were used. The t-test with Welch's correction served as the parametric test, while the Mann-Whitney test was applied for nonparametric data. Two way ANOVA was used for timeline comparison between strains readouts when indicated. Data are presented as

mean ± standard error of the mean. $P < 0.05$ was considered statistically significant. All analyses were conducted with GraphPad Prism 8 software.

RESULTS

PKR but not GCN2 regulates sensorimotor recovery after sciatic nerve crush.

Sensorimotor function strongly depends on maintaining or recovering axonal density in peripheral nerves and on specific proteome elements that support axo-glial interactions [86, 134–141], neurotransmission efficiency [86, 142, 143], and coordination with innervation or sensory targets [85, 135, 144–148]. Interestingly, PKR has been reported to regulate the efficiency of neurotransmission under both physiological and stress conditions [149–153]. Additionally, GCN2 modulates myelination, a readout of axo-glial interaction [154, 155]. Thus, these ISR kinases may fine-tune proteostasis and contribute to the functional recovery of the sciatic nerve after injury. To investigate this possibility, we used loss-of-function (LOF) models of these kinases. We performed sciatic nerve crush and sham-control injuries on the posterior hindlimbs of PKR-KO and GCN2-KO mice and compared their sensorimotor performance with WT controls under the same conditions (Fig. 1A). Motor function was evaluated using the clasping test (see Methods) at 1, 3, 7, 14, and 21 DPI (Fig. 1B). At 1 DPI, PKR-KO and GCN2-KO mice exhibited significantly lower hindlimb clasping test scores than sham animals (Fig. 1C-D). At 3 DPI, PKR-KO mice exhibited a slight recovery in the clasping test score that was indistinguishable from WT mice (Fig. 1C). In contrast, GCN2-KO mice showed higher clasping test scores than WT mice at the same DPI (Fig. 1D), suggesting that the initiation of motor recovery differentially depends on PKR and GCN2. From 7 DPI to 21 DPI, PKR-KO mice exhibited significantly lower hindlimb clasping test scores than WT animals (Fig. 1C). To further characterize this phenotype, we analyzed the components of the clasping score separately (limb extension and digit extension). The reduced scores observed in PKR-KO mice were mainly attributable to impaired limb extension (Supplementary Fig. 1A-B). In contrast, GCN2-KO mice showed motor recovery in clasping scores that was indistinguishable from WT during this time window (Fig. 1D, Supplementary Fig. 1C-D). Notably, the contralateral sham hindlimb of PKR-KO mice also showed a significant decline in clasping score from 1 to 21 DPI compared with WT sham controls (Fig. 1C). Together, these results demonstrate that PKR plays a major role in the recovery of peripheral nerve-dependent sensorimotor function after injury.

Given the altered motor recovery observed in PKR-KO mice after injury, we next examined whether structural changes in the peripheral nerve accompanied this phenotype. We therefore assessed the contribution of PKR and GCN2 to nerve structure during degeneration and regeneration by quantifying axonal densities in the LOF models (Fig. 1E). Axonal density (axons/100μm^2) was quantified in immunofluorescence images detecting NF-H, as an axonal marker, in transverse sections of sciatic nerves distal to the injury from WT, GCN2-KO, and PKR-KO mice at stages when axonal degeneration (3 DPI) and regeneration (21 DPI) occur extensively. We observed a significant decrease in axonal density at 3 DPI in both PKR-KO and GCN2-KO nerves compared with their respective sham counterparts (Fig. 1F-G). By 21 DPI, however, axonal densities in both PKR-KO and GCN2-KO sciatic nerves recovered

to levels comparable to their sham nerves (Fig. 1F-G). Moreover, axonal densities in PKR-KO or GCN2-KO nerves at sham, 3 DPI, or 21 DPI were indistinguishable from WT (Fig. 1F-G). These results indicate that loss of PKR or GCN2 does not significantly affect the mechanisms regulating axonal density during key stages of nerve degeneration and regeneration. Altogether, our results suggest that PKR regulates sensorimotor recovery independently of axonal density restoration. These observations raise the possibility that subtler peripheral nerve features or regulatory inputs from central nervous system circuits contribute to the observed phenotype. Based on this, we next assessed the local morphological and functional status of the peripheral nerve in PKR-KO mice after injury.

PKR contributes to the functional recovery of the injured sciatic nerve.

To evaluate the contribution of PKR to the functional recovery of the peripheral nerve through localized mechanisms, we analyzed sensorimotor function specifically in the crushed hindlimb of PKR-KO mice using a functional index that primarily reflects peripheral nerve status. We measured the Sciatic Functional Index (SFI), which evaluates only hindlimb footprint patterns, in crushed PKR-KO mice at the same time points after injury and compared the results with WT controls (Fig. 2A). At 1 DPI, both groups exhibited a similar and significant reduction in SFI (Fig. 2B). However, during the recovery phase (3–14 DPI), PKR-KO mice consistently showed lower SFI values than WT mice (Fig. 2B). By 21 DPI, SFI values in PKR-KO mice had recovered to levels indistinguishable from those of WT mice (Fig. 2B). These results indicate that the functional recovery of the sciatic nerve is delayed in PKR-KO mice. Furthermore, this impairment affects functional parameters that strongly depend on the local morphological and functional status of the peripheral nerve.

Based on this, we further examined the structural integrity of the sciatic nerve during degeneration and regeneration. To this end, we performed a qualitative histological analysis of axonal and myelin structures along the sciatic nerve at 3 DPI (during degeneration) and at 21 DPI (regeneration) in WT and PKR-KO mice (Fig. 2C). Whole longitudinal segments of the sciatic nerves (3 mm) were collected, and distal regions were compared in terms of the morphology and spatial distribution of axons and myelin ovoids (Fig. 2C). We found that WT and PKR-KO nerves consistently showed similar histological patterns across the analyzed time points (Fig. 2C). These observations suggest that the progression and morphological features of structural changes in the sciatic nerve after crush are not significantly affected by PKR deficiency. Of note, we also examined sensory function by measuring the 50% withdrawal threshold to mechanical stimulation (Von Frey test) in the crushed hindlimb of PKR-KO mice and compared it with crushed WT controls. Both genotypes exhibited an indistinguishable pattern of complete loss of withdrawal threshold from 1 to 7 DPI after injury (Supplementary Fig. 2A). This was followed by progressive recovery of sensory responses, with withdrawal thresholds returning to baseline by 21 DPI in both genotypes (Supplementary Fig. 2A). Notably, at 14 DPI, a higher proportion of PKR-KO mice responded to mechanical stimulation compared with WT mice (Supplementary Fig. 2B). Among responding animals, PKR-KO mice also displayed significantly higher withdrawal thresholds than responding WT mice (Supplementary Fig. 2B).

Altogether, these findings identify PKR as a key regulator of peripheral nerve-dependent sensorimotor recovery after injury, while indicating that the functional deficits observed in PKR deficiency occur despite normal axon density restoration and preserved overall nerve structure.

Activation Dynamics of the ISR in the Sciatic Nerve After Injury.

Since the ISR pathway is activated in response to changes in intracellular conditions and promotes cellular adaptation [120, 156–158], we first asked whether the ISR is triggered during the adaptation of peripheral nerves to an acute injury process that involves extensive degeneration followed by regeneration. During this process, levels of neuronal and glial marker proteins decrease and may recover depending on the severity of damage [159–161]. To investigate this, we analyzed the abundance and activation patterns of the ISR core in sciatic nerves at 3, 7, 14, or 21 days post-injury (DPI). We focused on the injury site (medial) and distal segments undergoing degeneration and regeneration, and compared them with undamaged control nerves (0 DPI) (Fig. 3A). Specifically, we measured levels of eIF2α and phosphorylated eIF2α (p-eIF2α) by Western blot in WT mouse sciatic nerve segments collected at the indicated time points (Fig. 3A). In parallel, levels of an axonal marker (Neurofilament Heavy chain, NF-H) and a myelination marker (myelin basic protein, MBP) were monitored in the same samples, as indicators of nerve integrity (Fig. 3A). As expected, distal segments of injured sciatic nerves exhibited significant and sustained axon loss, indicated by decreased NF-H and MBP levels after injury (Fig. 3B). Compared with non-injured WT nerves, NF-H levels decreased by about 80% starting at 3 DPI and remained reduced until 14 DPI in distal sciatic nerve segments after crush (Fig. 3B). Concomitantly, MBP levels declined sharply by approximately 90% at 7 DPI, becoming nearly undetectable, and remaining low until 21 DPI in the same samples (Fig. 3B). Notably, the combined decrease in NF-H and MBP observed at 7 DPI coincided with increased levels of ISR activity (Fig. 3B-C). Specifically, both eIF2α and p-eIF2α significantly increased at 7 DPI and remained elevated until 14 DPI in distal sciatic nerve segments after crush (Fig. 3C). Notably, total and phosphorylated eIF2α levels varied synchronously along the post-injury timeline (Fig. 3C). Based on this observation, subsequent analyses of ISR activity considered both protein forms.

Restoration of the axonal marker NF-H in sciatic nerves after a crush injury has been widely reported [159–161]. The final time point in our analysis allowed us to examine whether changes in ISR activity coincided with axonal marker recovery. NF-H levels recovered at 21 DPI and increased by 30% compared with their lowest levels at 3 DPI in distal WT sciatic nerve segments after crush (Fig. 3B). Notably, at this same time point, eIF2α and p-eIF2α levels became indistinguishable from those observed in intact nerves (Fig. 3C). Thus, the recovery of axonal marker levels coincided with a decrease in ISR activity.

At the injury site, crush induces axonal transection, generating axonal stumps connected to the neuronal soma and distal disconnected segments [33, 85, 162–170]. This region is characterized by altered intracellular conditions, including increased ROS and calcium levels, which are known to activate the ISR [63, 64, 66, 88, 171–178]. Consistent with this, eIF2α and p-eIF2α showed an early increase at 3 DPI and were significantly elevated from 7 to 21 DPI in medial nerve segments (Supplementary Fig. 3A-B). These

results indicate that nerve crush induces a rapid and persistent ISR response that extends beyond the injury site.

These observations reveal that sciatic nerve injury triggers a spatially and temporally structured ISR activation pattern along the injured nerve that coincides with functional loss and recovery. Our results support the idea that appropriate temporal regulation of ISR activity may be associated with successful nerve degeneration and regeneration.

Building on these findings, we examined PKR-mediated ISR activation by assessing eIF2α and p-eIF2α levels together with NF-H and the myelination marker MBP, as well as markers of axonal integrity and myelination in sciatic nerve segments from PKR-KO mice collected at the injury site and in the distal region after the crush (Fig. 3D). In distal nerve segments, NF-H and MBP patterns differed from those observed in WT mice (Fig. 3E). NF-H levels in PKR-KO nerves failed to return to basal levels as observed in WT animals, while MBP levels dropped drastically at 3 DPI (Fig. 3E). Regarding ISR activation, PKR-KO nerves displayed a temporal pattern that differed markedly from WT animals. Phosphorylated eIF2α levels peaked at 3 DPI and returned to baseline by 7 DPI in the distal-to-crush region (Fig. 3F). Total eIF2α levels also peaked at 3 DPI, but unlike WT mice, exhibited a second peak at 21 DPI (Fig. 3F). Together, these results indicate that loss of PKR disrupts the temporal architecture of ISR activation after nerve injury, revealing that PKR shapes the adaptive stress response accompanying peripheral nerve degeneration and regeneration.

Differences in ISR activation under PKR deficiency.

Next, we asked whether specific differences in ISR activation or nerve integrity markers could be detected at defined time points after injury in the absence of PKR. To address this, we compared NF-H, MBP, eIF2α, and p-eIF2α levels between PKR-KO and WT mice in distal nerve segments at time points covering the degenerative (Fig. 4) and regenerative (Fig. 5) phases after injury. We found no differences in eIF2α, p-eIF2α, and MBP levels between intact PKR-KO and WT sciatic nerves (Fig. 4A). In contrast, NF-H levels were significantly higher in PKR-KO intact nerves (Fig. 4A), indicating that PKR partially modulates the basal composition of the sciatic nerve. At 3 DPI, eIF2α levels were higher in distal PKR-KO nerve segments compared with WT, while no differences were detected in the other proteins analyzed (Fig. 4B). At 7 DPI, eIF2α levels were lower and MBP levels were higher in PKR-KO distal segments compared with WT (Fig. 5A). At 14 DPI, p-eIF2α levels were reduced in PKR-KO nerves (Fig. 5B), whereas no differences were observed at 21 DPI (Fig. 5C). In all time points analyzed, no differences were found in the p-eIF2α/eIF2α ratio (Supplementary Fig. 6A). Together, these results indicate that PKR modulates specific protein abundances during both degenerative stress and regeneration, with partial overlap between ISR activation dynamics and MBP changes.

At the injury site, no differences were detected at 3, 7, or 14 DPI, whereas lower eIF2α and p-eIF2α levels were observed at 21 DPI in PKR-KO sciatic nerves compared with WT (Supplementary Figs. 4–5). Notably, at 7 DPI, the p-eIF2α/eIF2α ratio was decreased in PKR-KO medial segments with respect to WT, revealing PKR-dependent ISR activation at this regenerative stage (Supplementary Fig. 6B). The elevated

NF-H levels observed in intact PKR-KO nerves were also detected in these samples (Supplementary Fig. 4A). Altogether, these results indicate that PKR regulates ISR activation dynamics at the injury site after crush. Moreover, PKR-dependent modulation of the ISR activity and nerve marker proteins appears to be region and time-specific.

Role of PKR in the Recovery of Sciatic Nerve Ultrastructure After Injury.

Sciatic nerves restore their ultrastructure after a crush injury [146, 179–182]. During this regenerative process, the abundances of both unmyelinated and myelinated axons are progressively replenished [179, 183, 184]. In parallel, the ultrafine structure of myelination is also re-established [92, 180, 181, 185–189], ultimately enabling restoration of sensorimotor function [132, 183, 190–194]. Conversely, defective ultrastructural recovery has been shown to contribute to delayed or incomplete functional recovery [112, 195–197]. Given these observations and our findings indicating that PKR regulates the structural and functional integrity of the sciatic nerve at potentially subtle levels, we asked whether PKR modulates ultrastructural recovery following crush injury. To address this, we assessed the abundance of myelinated axons and their degree of myelination at 21 DPI, a time point at which PKR-dependent motor dysfunction is observed after injury (Fig. 6). Using quantitative electron microscopy, we measured the numerical density of myelinated axons (axons/μm^2) and calculated the g-ratios in sham and distal-to-crush sciatic nerve segments from PKR-KO mice at 21 DPI and compared these to WT nerves (Fig. 6C-D). These values were also compared with sham sciatic nerve controls (Fig. 6C-D). We found that the numerical density of myelinated axons at 21 DPI was reduced in distal-to-crush PKR-KO nerve segments compared with sham controls, an effect not observed in WT nerves (Fig. 6C). In addition, regenerated PKR-KO nerves displayed significantly higher g-ratios compared with WT nerves (Fig. 6D), indicating an altered relationship between axonal diameter and myelin thickness.

Overall, our results indicate that PKR shapes ISR activation dynamics in injured sciatic nerves and contributes to the restoration of axonal ultrastructure and motor function during peripheral nerve regeneration.

DISCUSSION

Peripheral nerve regeneration requires coordinated structural remodeling and restoration of neuronal function, processes that depend on tight regulation of protein homeostasis. Here, we identify the ISR kinase PKR as a key regulator that links stress signaling to peripheral nerve structural and functional recovery after injury. Together, these findings indicate that the temporal dynamics of ISR activation is crucial for successful peripheral nerve degeneration and regeneration. Through combining temporal and spatial analyses of ISR activation with morphological and behavioral assessments, we found that ISR activation follows a specific temporal pattern after nerve injury. It increases during the initial degenerative phase and returns to baseline during regeneration, in close synchrony with axonal and myelin remodeling: after injury, ISR activation rises as myelin levels decrease, and ISR downregulation coincides with the recovery of axonal markers (Fig. 3A). This temporal pattern of ISR activation is

detectable at the injury site (Fig. 2C, Supplementary Fig. 3A) and in distal nerve regions undergoing degeneration and regeneration (Fig. 3A). PKR deficiency alters this pattern of ISR activation (Fig. 3B), disrupts the recovery of axonal proteins (Fig. 3B), impairs recovery of motor (Fig. 1B-C, 2A-B) and sensory functions (Supplementary Fig. 2), and affects nerve structure (Fig. 6) after the crush. These results demonstrate that PKR modulates the fine-tuning of the nerve proteome necessary for structural and functional nerve regeneration. Peripheral nerve injury induces extensive alterations in the intracellular environment, including increased calcium levels, oxidative stress, metabolic imbalance, and the accumulation of damage-associated RNA species [63, 64, 66, 88, 171–178, 198], all of which are known to activate ISR kinases [156, 199, 200]. Consistently, we found that eIF2α phosphorylation increases after a crush injury (7 DPI) and remains elevated in WT distal nerve segments (Fig. 3A), where axonal degeneration and Schwann cell demyelination occur [68, 95, 170, 201–203]. This pattern of eIF2α phosphorylation strongly suggests that ISR activity plays a role in peripheral nerve degeneration after injury. In fact, we found that PKR-KO distal nerve segments exhibited lower MBP levels at earlier time points after injury than WT nerves, whereas NF-H levels did not recover similarly to WT nerves (Fig. 3B). These results suggest that PKR regulates the timing of demyelination following nerve injury and the dynamics of recovery of axonal integrity. In contrast, previous reports indicate that Schwann cell dedifferentiation, demyelination, and cytoskeletal reorganization are required to execute the fragmentation of their associated axons when reported by NF-H [37]. Considering this, PKR could mediate myelin processing in a way that modifies this previously described axo-glial interaction.

The activation of the ISR at both nerve regions, at the injury site and distal to the injury (4 mm apart), suggests that the ISR extends along the nerve, reaching areas where stress-related disruptions and diverse phenotypic cellular changes have been reported [37, 63, 66, 68, 95, 170, 201–203]. In WT animals, ISR activity decreased to baseline levels by 21 DPI, coinciding with the reappearance of axonal (NF-H) markers in distal injury nerve segments (Fig. 3A). In contrast, PKR-KO nerves displayed an early (3 DPI) but very short-lived significant increase in ISR activation at the region distal to injury (Fig. 3B). Interestingly, this earlier phosphorylation of eIF2α in PKR-KO nerves also occurs at injury sites (Supplementary Fig. 3B). This suggests that, after transient PKR-dependent ISR activation, the suppression of ISR activity promotes proteome remodeling during nerve regeneration, and this phosphorylation of eIF2α is managed similarly at both the distal and injury sites. Furthermore, while WT nerves display eIF2α levels comparable to their respective sham controls at 21 DPI (Fig. 3A), PKR-KO nerve segments distal to the injury show significantly higher (13-fold higher) levels (Fig. 3D-E), supporting the idea that PKR regulates eIF2α levels, as previously reported [204], and that the loss of this control could be part of the regulation executed by PKR in the adaptive response to nerve regeneration. PKR is one of the four kinases found in axons [129, 205, 206] that integrate their signaling into eIF2α. Our results suggest that its absence likely disrupts the overall capacity to sense stress signals in this tissue after injury. The ISR activation pattern detected in PKR-KO nerves indicates that a compensatory ISR activation is acting, but it is insufficient to promote the translational and transcriptional programs required to reestablish cellular homeostasis after injury. Altogether, these observations suggest that PKR

orchestrates the amplitude, persistence, and adaptive effects of ISR activation that occurs at the transition from degeneration to regeneration.

Our comparative results on axonal density and sensorimotor analysis after sciatic nerve injury indicate that PKR plays a particular, non-redundant role among ISR kinases during peripheral nerve regeneration. Interestingly, nerves from GCN2-KO or PKR-KO mice exhibited axonal density dynamics indistinguishable from those of WT (Fig. 1E), indicating that deficiencies in either kinase do not disrupt the process of axonal degeneration that enables complete axonal repopulation. However, when motor performance was evaluated, GCN2-KO mice behaved similarly to WT mice (Fig. 1D), whereas PKR-KO mice showed delayed and incomplete recovery of clasping ability (Fig. 1C). This suggests that PKR is required for regenerative events necessary to restore this motor function. Notably, the motor performance of the PKR-KO mice on the contralateral sham limb was also lower than WT sham (Fig. 1C). It has been reported that, following sciatic nerve constriction or ligation, PKR is activated in the rat's spinal cord and brain [207]. Altogether, this suggests that PKR can negatively regulate the propagation of motor dysfunction from the directly stressed peripheral nerves to other intact peripheral nerve tracts. These results strongly suggest that PKR is a major regulator of motor function recovery.

Sensory recovery followed a comparable trajectory between genotypes, with only minor differences at DPI 14 (Supplementary Fig. 2A). PKR-KO recovers touch response at DPI 14 (7 responders), and those who respond have higher (50%) withdrawal response to touch in comparison to WT responders (5 responders) (Supplementary Fig. 2B). At this same time point, PKR-KO injury site and distal to crush nerve segments have significantly lower levels of ISR activity (Supplementary Fig. 3C and Fig. 3D). Interestingly, active PKR (p-PKR) has been reported in both peripheral motor myelinated and unmyelinated fibers, mostly sensory [208]. Furthermore, sciatic nerve stress induced by constriction (without axonal degeneration) is enough to produce an activated PKR-dependent neuropathic pain [208]. Also, pharmacological inhibition of PKR or eIF2α modulates thermal sensitivity [209]. Altogether, these sensory performance results suggest that PKR plays a role in sensorial function via eIF2α and p-eIF2α. These observations suggest that PKR-dependent signaling may preferentially influence motor axon fine structure and myelination, processes that require sustained protein synthesis [13, 16, 21, 210–213] and axo-glial coordination [25, 35, 93, 115, 214–219]. The mild sensory differences (Supplementary Fig. 2A) might reflect a lower dependence on the structural demands of unmyelinated fibers in PKR.

Our time-point-to-time-point analysis at distal-to-injury nerve segments allowed us to compare the fine regulation of PKR over nerve and ISR proteins during the recovery of the nerve phenotype after injury. We found that in sham nerves, PKR deficiency leads to elevated NF-H levels in sciatic nerves without affecting ISR activity or myelin protein abundance (Fig. 4A), indicating a PKR-dependent imbalance in the axonal cytoskeleton. After injury, PKR regulates eIF2α levels in degenerating and regenerating nerve segments. By 7 DPI, PKR-deficient mice do not show the expected decrease in myelin (Fig. 5A). Axons are degenerating at this time point, which activates demyelination, dedifferentiation, and Schwann cell proliferation [66, 95, 220, 221]. The observed decrease in eIF2α levels at this point in PKR-KO nerves may also reflect PKR-dependent regulation in non-neuronal cells, such as Schwann cells. Thus, ISR signaling

appears essential for coordinating proteostasis and resource allocation during peripheral nerve remyelination.

Based on our results indicating altered remyelination, we explored nerve ultrastructure in PKR-KO mice at distal-to-injury regenerated nerve segments (21 DPI) and compared them with WT. At 21 DPI, PKR-KO nerves showed a reduced numerical density of myelinated axons (Fig. 6B), with no difference observed in unmyelinated axon abundance (data not shown). This differential effect on myelinated versus unmyelinated axons aligns with the strong and persistent motor dysfunction we found here (Fig. 1), which is mainly mediated by myelinated axons, and the mild impact on sensory function, mainly mediated by unmyelinated axons. Interestingly, slower regeneration of myelinated axons has been reported in WT aged mice compared to young ones [179]. Based on this, we assayed whether regenerated myelinated axons in PKR-KO nerves have phenotypes associated with slower or incomplete maturation. We found that myelinated axons in PKR-KO-regenerated nerves had a higher g-ratio at 21 DPI. These findings indicate that PKR plays a role in the proper structural maturation of nerves. One aspect of PKR's involvement in fine nerve structure maturation may be its role in promoting recovery of NF-H levels at 21 DPI post-injury, as shown in Fig. 3. Furthermore, previous studies have shown that ISR activity (phosphorylation of eIF2α) is necessary for MBP-based remyelination. Considering this, the decreased ISR activity in PKR-KO regenerating nerves that we observed (Fig. 3B) may contribute to the defective remyelination we found. These ultrastructural alterations also suggest that PKR signaling is required for proteostatic regulation during timed and extended remyelination of Schwann cells. In these cells, eIF2α phosphorylation regulates the synthesis of myelin proteins and lipid metabolism [128]. Therefore, the premature decline in ISR activity observed in PKR-KO mice (Fig. 3B) may also impair the transcriptional and translational programs that support myelin assembly. Together, these data place PKR-dependent ISR signaling as a fine-tuning mechanism for myelination, involved on its proper resource allocation during regeneration.

Despite the widespread use of the PKR genetic deficiency model, which allows the identification of anatomical and temporal contexts in which multiple adaptive cellular events must occur for degeneration or regeneration, this same feature also poses a caveat for understanding the role of local proteostatic activities during these processes. Further research is needed to clarify these local dynamics.

The ISR links stress sensing and proteome remodeling by transiently repressing global translation while promoting the translation of specific mRNAs [118, 120]. In peripheral nerves, this mechanism likely supports axonal maintenance and repair. Our data suggest a dimorphic effect in which PKR-driven ISR activation limits nerve stress during degeneration, followed in sequence by timely deactivation to enable translation reinitiation, cytoskeletal rebuilding, and remyelination. In PKR-KO, disruption of this sequence leads to maladaptive responses and impaired structural and functional recovery. These findings highlight that ISR timing and its corresponding adaptative effect, rather than absolute pathway activation, determines successful regeneration, positioning PKR as a critical orchestrator governing nerve repair.

In summary, our results demonstrate that PKR shapes the temporal dynamics, spatial distribution, and regenerative effects of the ISR after peripheral nerve injury, sustaining eIF2α phosphorylation during degeneration to enable adaptive proteome remodeling, supporting myelin restoration and motor function recovery. To our knowledge, the role of the PKR-eIF2α axis in progression is one of the first identified proteostatic mechanisms to modulate peripheral nerve structure and function as a key factor during the degenerative and regenerative phases after injury. Targeting PKR-dependent ISR pathways could offer a therapeutic standpoint to modulate nerve regeneration. Fine-tuning PKR activity or ISR intensity may improve repair without impairing stress resilience, highlighting the importance of defining the temporal window in which PKR supports regeneration.

Declarations

Author Contributions: Conceptualization, S.M, N.W.M, C.M.M.; Investigation, N.W.M., C.M.M., A.T., I.S.P., D.B.; Formal analysis, N.W.M, C.M.M., S.M.; Writing—original draft preparation, S.M., N.W.M., C.M.M.; Writing—Review and Editing, N.W.M, S.M.; M.C. Supervision, S.M.; Project Administration, S.M.; Funding acquisition, S.M., and N.M.W.

All authors have read and agreed to the published version of the manuscript.

Funding: This work was supported by the National Agency of Research and Development (ANID): “Financiamiento Basal para Centros Científicos y Tecnológicos de Excelencia Centro Ciencia & Vida” FB210008 (S.M); FONDECYT ANID 1230334 (S.M.); FONDECYT ANID 1220823 (M.C.); FONDAP/15150012 (S.M.).

Availability of Data and Material: The datasets used and/or analyzed during this current study are available from the corresponding author upon reasonable request.

Acknowledgments: We thank the animal facility at FCV/Universidad San Sebastián and the “Unidad de Microscopía Avanzada” (UMA) at Pontificia Universidad Católica, Santiago, Chile, for the electron microscopy work.

Competing Interest: N.W.M., C.M.M., A.T., I.S.P., D.B., M.C. and S.M. declare that they have no competing interests.

Ethics Approval: All studies were conducted in accordance with the eighth edition of the Guide for the Care and Use of Laboratory Animals. The experimental protocols, including those involving anesthesia, pain, distress, and euthanasia (No P034/2022, the ethical approval date was May 13, 2022), were approved by the IACUC at the FCV.

Consent for Publication: Not applicable.

References

1. Kalambogias, J. and Y. Yoshida, *Converging integration between ascending proprioceptive inputs and the corticospinal tract motor circuit underlying skilled movement control.* Curr Opin Physiol, 2021. **19**: p. 187-193.
2. Duff, S.V., *Impact of peripheral nerve injury on sensorimotor control.* J Hand Ther, 2005. **18**(2): p. 277-91.
3. Crago, P.E., *Neuromodulation by combined sensory and motor stimulation in the peripheral nerve: tendon organ afferent activity.* J Neural Eng, 2019. **16**(1): p. 016015.
4. Plant, G.W., J.A. Weinrich, and J.A. Kaltschmidt, *Sensory and descending motor circuitry during development and injury.* Curr Opin Neurobiol, 2018. **53**: p. 156-161.
5. Nielsen, J.B., *Sensorimotor integration at spinal level as a basis for muscle coordination during voluntary movement in humans.* Journal of Applied Physiology, 2004. **96**(5): p. 1961-1967.
6. Asan, A.S., J.R. McIntosh, and J.B. Carmel, *Targeting Sensory and Motor Integration for Recovery of Movement After CNS Injury.* Front Neurosci, 2021. **15**: p. 791824.
7. Abraira, V.E. and D.D. Ginty, *The sensory neurons of touch.* Neuron, 2013. **79**(4): p. 618-39.
8. Jessen, K.R. and R. Mirsky, *The origin and development of glial cells in peripheral nerves.* Nat Rev Neurosci, 2005. **6**(9): p. 671-82.
9. Kanda, T., et al., *Morphological changes in unmyelinated nerve fibres in the sural nerve with age.* Brain, 1991. **114 (Pt 1B)**: p. 585-99.
10. Carlsen, F. and F. Behse, *Three dimensional analysis of Schwann cells associated with unmyelinated nerve fibres in human sural nerve.* J Anat, 1980. **130**(Pt 3): p. 545-57.
11. Behse, F., et al., *Unmyelinated fibres and Schwann cells of sural nerve in neuropathy.* Brain, 1975. **98**(3): p. 493-510.
12. Pfeiffer-Guglielmi, B., et al., *Axonal and dendritic localization of mRNAs for glycogen-metabolizing enzymes in cultured rodent neurons.* BMC Neurosci, 2014. **15**: p. 70.
13. Wu, S., et al., *Insight into protein synthesis in axon regeneration.* Exp Neurol, 2023. **367**: p. 114454.
14. Jung, H., B.C. Yoon, and C.E. Holt, *Axonal mRNA localization and local protein synthesis in nervous system assembly, maintenance and repair.* Nat Rev Neurosci, 2012. **13**(5): p. 308-24.
15. Dalla Costa, I., et al., *The functional organization of axonal mRNA transport and translation.* Nat Rev Neurosci, 2021. **22**(2): p. 77-91.
16. Terenzio, M., et al., *Locally translated mTOR controls axonal local translation in nerve injury.* Science, 2018. **359**(6382): p. 1416-1421.
17. Obara, I. and S.P. Hunt, *Axonal protein synthesis and the regulation of primary afferent function.* Dev Neurobiol, 2014. **74**(3): p. 269-78.
18. Cox, L.J., et al., *Intra-axonal translation and retrograde trafficking of CREB promotes neuronal survival.* Nat Cell Biol, 2008. **10**(2): p. 149-59.
19. Yoo, S., et al., *Dynamics of axonal mRNA transport and implications for peripheral nerve regeneration.* Exp Neurol, 2010. **223**(1): p. 19-27.

20. Court, F.A., et al., *Schwann cell to axon transfer of ribosomes: toward a novel understanding of the role of glia in the nervous system.* J Neurosci, 2008. **28**(43): p. 11024-9.
21. Spaulding, E.L. and R.W. Burgess, *Accumulating Evidence for Axonal Translation in Neuronal Homeostasis.* Front Neurosci, 2017. **11**: p. 312.
22. Patel, P., et al., *Intra-axonal translation of Khsrp mRNA slows axon regeneration by destabilizing localized mRNAs.* Nucleic Acids Res, 2022. **50**(10): p. 5772-5792.
23. Holt, C.E. and E.M. Schuman, *The central dogma decentralized: new perspectives on RNA function and local translation in neurons.* Neuron, 2013. **80**(3): p. 648-57.
24. Yao, X., et al., *Schwann cell-secreted frizzled-related protein 1 dictates neuroinflammation and peripheral nerve degeneration after neurotrauma.* Cell Rep Med, 2024. **5**(11): p. 101791.
25. Lopez-Leal, R. and F.A. Court, *Schwann Cell Exosomes Mediate Neuron-Glia Communication and Enhance Axonal Regeneration.* Cell Mol Neurobiol, 2016. **36**(3): p. 429-36.
26. van Erp, S., et al., *Age-related loss of axonal regeneration is reflected by the level of local translation.* Exp Neurol, 2021. **339**: p. 113594.
27. Brushart, T.M., et al., *Schwann cell phenotype is regulated by axon modality and central-peripheral location, and persists in vitro.* Exp Neurol, 2013. **247**: p. 272-81.
28. Hoke, A., et al., *Schwann cells express motor and sensory phenotypes that regulate axon regeneration.* J Neurosci, 2006. **26**(38): p. 9646-55.
29. Liao, S., et al., *The phenotypic changes of Schwann cells promote the functional repair of nerve injury.* Neuropeptides, 2024. **106**: p. 102438.
30. Court, F.A. and J. Alvarez, *Local regulation of the axonal phenotype, a case of merotrophism.* Biol Res, 2005. **38**(4): p. 365-74.
31. Alvarez, J., A. Giuditta, and E. Koenig, *Protein synthesis in axons and terminals: significance for maintenance, plasticity and regulation of phenotype. With a critique of slow transport theory.* Prog Neurobiol, 2000. **62**(1): p. 1-62.
32. Alvarez, J., *The autonomous axon: a model based on local synthesis of proteins.* Biol Res, 2001. **34**(2): p. 103-9.
33. Beirowski, B., et al., *The progressive nature of Wallerian degeneration in wild-type and slow Wallerian degeneration (WldS) nerves.* BMC Neurosci, 2005. **6**: p. 6.
34. Verheijen, M.H., et al., *Increased axonal ribosome numbers is an early event in the pathogenesis of amyotrophic lateral sclerosis.* PLoS One, 2014. **9**(1): p. e87255.
35. Stassart, R.M. and A. Woodhoo, *Axo-glial interaction in the injured PNS.* Dev Neurobiol, 2021. **81**(5): p. 490-506.
36. Beirowski, B., *Emerging evidence for compromised axonal bioenergetics and axoglial metabolic coupling as drivers of neurodegeneration.* Neurobiol Dis, 2022. **170**: p. 105751.
37. Catenaccio, A., et al., *Molecular analysis of axonal-intrinsic and glial-associated co-regulation of axon degeneration.* Cell Death Dis, 2017. **8**(11): p. e3166.

38. Starobova, H. and I. Vetter, *Pathophysiology of Chemotherapy-Induced Peripheral Neuropathy.* Front Mol Neurosci, 2017. **10**: p. 174.
39. Muramatsu, K., *Diabetes Mellitus-Related Dysfunction of the Motor System.* Int J Mol Sci, 2020. **21**(20).
40. Wang, Y., et al., *Decreased peripheral nerve damage after ischemia-reperfusion injury in mice lacking TNF-alpha.* J Neurol Sci, 2008. **267**(1-2): p. 107-11.
41. Jortner, B.S., *Nerve Fiber Regeneration in Toxic Peripheral Neuropathy.* Toxicol Pathol, 2020. **48**(1): p. 144-151.
42. Bhattacharya, M.R., et al., *A model of toxic neuropathy in Drosophila reveals a role for MORN4 in promoting axonal degeneration.* J Neurosci, 2012. **32**(15): p. 5054-61.
43. Bennett, G.J., et al., *Terminal arbor degeneration--a novel lesion produced by the antineoplastic agent paclitaxel.* Eur J Neurosci, 2011. **33**(9): p. 1667-76.
44. Lauria, G., et al., *Axonal swellings predict the degeneration of epidermal nerve fibers in painful neuropathies.* Neurology, 2003. **61**(5): p. 631-6.
45. Peters, O.M., et al., *Genetic diversity of axon degenerative mechanisms in models of Parkinson's disease.* Neurobiol Dis, 2021. **155**: p. 105368.
46. Kurowska, Z., et al., *Is Axonal Degeneration a Key Early Event in Parkinson's Disease?* J Parkinsons Dis, 2016. **6**(4): p. 703-707.
47. Moss, K.R. and A. Hoke, *Targeting the programmed axon degeneration pathway as a potential therapeutic for Charcot-Marie-Tooth disease.* Brain Res, 2020. **1727**: p. 146539.
48. Linnemann, C., et al., *Peripheral Neuropathy in Spinocerebellar Ataxia Type 1, 2, 3, and 6.* Cerebellum, 2016. **15**(2): p. 165-73.
49. Gentile, F., et al., *The Peripheral Nervous System in Amyotrophic Lateral Sclerosis: Opportunities for Translational Research.* Front Neurosci, 2019. **13**: p. 601.
50. McCray, B.A. and S.S. Scherer, *Axonal Charcot-Marie-Tooth Disease: from Common Pathogenic Mechanisms to Emerging Treatment Opportunities.* Neurotherapeutics, 2021. **18**(4): p. 2269-2285.
51. Salvadores, N., et al., *Axonal Degeneration during Aging and Its Functional Role in Neurodegenerative Disorders.* Front Neurosci, 2017. **11**: p. 451.
52. Li, H., et al., *Huntingtin aggregate-associated axonal degeneration is an early pathological event in Huntington's disease mice.* J Neurosci, 2001. **21**(21): p. 8473-81.
53. Lopez-Grancha, M., et al., *A Novel Selective PKR Inhibitor Restores Cognitive Deficits and Neurodegeneration in Alzheimer Disease Experimental Models.* J Pharmacol Exp Ther, 2021. **378**(3): p. 262-275.
54. Barnes, S.L., T.A. Miller, and N.G. Simon, *Traumatic peripheral nerve injuries: diagnosis and management.* Curr Opin Neurol, 2022. **35**(6): p. 718-727.
55. Valentine, W.M., *Toxic Peripheral Neuropathies: Agents and Mechanisms.* Toxicol Pathol, 2020. **48**(1): p. 152-173.

56. Weber, F. and A. Ziegler, *Axonal neuropathy in chronic peripheral arterial occlusive disease.* Muscle Nerve, 2002. **26**(4): p. 471-6.
57. Teunissen, L.L., N.C. Notermans, and J.H. Wokke, *Relationship between ischemia and neuropathy.* Eur Neurol, 2000. **44**(1): p. 1-7.
58. Gargareta, V.I., et al., *Myelinated peripheral axons are more vulnerable to mechanical trauma in a model of enlarged axonal diameters.* Glia, 2024. **72**(9): p. 1572-1589.
59. Conforti, L., J. Gilley, and M.P. Coleman, *Wallerian degeneration: an emerging axon death pathway linking injury and disease.* Nat Rev Neurosci, 2014. **15**(6): p. 394-409.
60. Coleman, M.P. and A. Hoke, *Programmed axon degeneration: from mouse to mechanism to medicine.* Nat Rev Neurosci, 2020. **21**(4): p. 183-196.
61. Canty, A.J., et al., *In vivo imaging of injured cortical axons reveals a rapid onset form of Wallerian degeneration.* BMC Biol, 2020. **18**(1): p. 170.
62. Ertürk, A., et al., *Disorganized microtubules underlie the formation of retraction bulbs and the failure of axonal regeneration.* J Neurosci, 2007. **27**(34): p. 9169-80.
63. Villegas, R., et al., *Calcium release from intra-axonal endoplasmic reticulum leads to axon degeneration through mitochondrial dysfunction.* J Neurosci, 2014. **34**(21): p. 7179-89.
64. Kline, R.A., et al., *Altered mitochondrial bioenergetics are responsible for the delay in Wallerian degeneration observed in neonatal mice.* Neurobiol Dis, 2019. **130**: p. 104496.
65. Coleman, M., *Axon degeneration mechanisms: commonality amid diversity.* Nat Rev Neurosci, 2005. **6**(11): p. 889-98.
66. Barrientos, S.A., et al., *Axonal degeneration is mediated by the mitochondrial permeability transition pore.* J Neurosci, 2011. **31**(3): p. 966-78.
67. Tricaud, N., et al., *Traumatic and Diabetic Schwann Cell Demyelination Is Triggered by a Transient Mitochondrial Calcium Release through Voltage Dependent Anion Channel 1.* Biomedicines, 2022. **10**(6).
68. Tricaud, N. and H.T. Park, *Wallerian demyelination: chronicle of a cellular cataclysm.* Cell Mol Life Sci, 2017. **74**(22): p. 4049-4057.
69. Gerdts, J., et al., *Axon Self-Destruction: New Links among SARM1, MAPKs, and NAD+ Metabolism.* Neuron, 2016. **89**(3): p. 449-60.
70. Viader, A., et al., *Aberrant Schwann cell lipid metabolism linked to mitochondrial deficits leads to axon degeneration and neuropathy.* Neuron, 2013. **77**(5): p. 886-98.
71. Arrazola, M.S., et al., *Axonal Degeneration Is Mediated by Necroptosis Activation.* J Neurosci, 2019. **39**(20): p. 3832-3844.
72. Gilley, J. and M.P. Coleman, *Endogenous Nmnat2 is an essential survival factor for maintenance of healthy axons.* PLoS Biol, 2010. **8**(1): p. e1000300.
73. de Leon, A., J. Gibon, and P.A. Barker, *NGF-Dependent and BDNF-Dependent DRG Sensory Neurons Deploy Distinct Degenerative Signaling Mechanisms.* eNeuro, 2021. **8**(1).

74. Maor-Nof, M., et al., *Axonal Degeneration Is Regulated by a Transcriptional Program that Coordinates Expression of Pro- and Anti-degenerative Factors.* Neuron, 2016. **92**(5): p. 991-1006.
75. Gordon, T., *Peripheral Nerve Regeneration and Muscle Reinnervation.* Int J Mol Sci, 2020. **21**(22).
76. Bradke, F., J.W. Fawcett, and M.E. Spira, *Assembly of a new growth cone after axotomy: the precursor to axon regeneration.* Nat Rev Neurosci, 2012. **13**(3): p. 183-93.
77. Lam, T.C., et al., *Peripheral Nerve Regeneration Reimagined: Cutting-Edge Biomaterials and Biotechnological Innovations.* Bioengineering (Basel), 2025. **12**(8).
78. Rigoni, M. and S. Negro, *Signals Orchestrating Peripheral Nerve Repair.* Cells, 2020. **9**(8).
79. Liu, J., et al., *Role of microtubule dynamics in Wallerian degeneration and nerve regeneration after peripheral nerve injury.* Neural Regen Res, 2022. **17**(3): p. 673-681.
80. Kulkarni, R., A. Thakur, and H. Kumar, *Microtubule Dynamics Following Central and Peripheral Nervous System Axotomy.* ACS Chem Neurosci, 2022. **13**(9): p. 1358-1369.
81. Costa, A.C., et al., *Axon-specific microtubule regulation drives asymmetric regeneration of sensory neuron axons.* Elife, 2025. **13**.
82. Yaniv, S.P., et al., *Developmental axon regrowth and primary neuron sprouting utilize distinct actin elongation factors.* J Cell Biol, 2020. **219**(5).
83. Ducommun Priest, M., et al., *Dynein promotes sustained axonal growth and Schwann cell remodeling early during peripheral nerve regeneration.* PLoS Genet, 2019. **15**(2): p. e1007982.
84. Verma, P., et al., *Axonal protein synthesis and degradation are necessary for efficient growth cone regeneration.* J Neurosci, 2005. **25**(2): p. 331-42.
85. Ma, C.H., et al., *Accelerating axonal growth promotes motor recovery after peripheral nerve injury in mice.* J Clin Invest, 2011. **121**(11): p. 4332-47.
86. Lim, E.F., et al., *AlphaB-crystallin regulates remyelination after peripheral nerve injury.* Proc Natl Acad Sci U S A, 2017. **114**(9): p. E1707-E1716.
87. Khaitin, A., *Calcium in Neuronal and Glial Response to Axotomy.* Int J Mol Sci, 2021. **22**(24).
88. Wang, N., et al., *Targeting CB1R Rewires Ca(2+)-Dependent Mitophagy to Promote Nerve Regeneration.* Theranostics, 2025. **15**(17): p. 8873-8896.
89. Smith, T.P., et al., *Intra-axonal mechanisms driving axon regeneration.* Brain Res, 2020. **1740**: p. 146864.
90. Spira, M.E., D. Benbassat, and A. Dormann, *Resealing of the proximal and distal cut ends of transected axons: electrophysiological and ultrastructural analysis.* J Neurobiol, 1993. **24**(3): p. 300-16.
91. Takenaka, T., et al., *Glycolytic System in Axons Supplement Decreased ATP Levels after Axotomy of the Peripheral Nerve.* eNeuro, 2023. **10**(3).
92. Belanger, E., et al., *In vivo evaluation of demyelination and remyelination in a nerve crush injury model.* Biomed Opt Express, 2011. **2**(9): p. 2698-708.
93. Borger, A., et al., *How miRNAs Regulate Schwann Cells during Peripheral Nerve Regeneration-A Systemic Review.* Int J Mol Sci, 2022. **23**(7).

94. Jessen, K.R. and R. Mirsky, *The repair Schwann cell and its function after nerve injury.* 2016.
95. Gomez-Sanchez, J.A., et al., *After Nerve Injury, Lineage Tracing Shows That Myelin and Remak Schwann Cells Elongate Extensively and Branch to Form Repair Schwann Cells, Which Shorten Radically on Remyelination.* J Neurosci, 2017. **37**(37): p. 9086-9099.
96. Chen, C.Z., et al., *Schwann cell remyelination of the central nervous system: why does it happen and what are the benefits?* Open Biol, 2021. **11**(1): p. 200352.
97. Kegler, K., et al., *Contribution of Schwann Cells to Remyelination in a Naturally Occurring Canine Model of CNS Neuroinflammation.* PLoS One, 2015. **10**(7): p. e0133916.
98. Kim, S., et al., *Schwann cell O-GlcNAcylation promotes peripheral nerve remyelination via attenuation of the AP-1 transcription factor JUN.* Proc Natl Acad Sci U S A, 2018. **115**(31): p. 8019-8024.
99. Nocera, G. and C. Jacob, *Mechanisms of Schwann cell plasticity involved in peripheral nerve repair after injury.* Cell Mol Life Sci, 2020. **77**(20): p. 3977-3989.
100. Lemaitre, D., et al., *Collateral Sprouting of Peripheral Sensory Neurons Exhibits a Unique Transcriptomic Profile.* Mol Neurobiol, 2020. **57**(10): p. 4232-4249.
101. Saifetiarova, J., et al., *Reorganization of Destabilized Nodes of Ranvier in βIV Spectrin Mutants Uncovers Critical Timelines for Nodal Restoration and Prevention of Motor Paresis.* J Neurosci, 2018. **38**(28): p. 6267-6282.
102. Dombrowski, M.A., et al., *Myelination and nodal formation of regenerated peripheral nerve fibers following transplantation of acutely prepared olfactory ensheathing cells.* Brain Res, 2006. **1125**(1): p. 1-8.
103. Radtke, C. and P.M. Vogt, *Peripheral nerve regeneration: a current perspective.* Eplasty, 2009. **9**: p. e47.
104. Allodi, I., E. Udina, and X. Navarro, *Specificity of peripheral nerve regeneration: interactions at the axon level.* Prog Neurobiol, 2012. **98**(1): p. 16-37.
105. Li, Y., et al., *SCG10 is required for peripheral axon maintenance and regeneration in mice.* J Cell Sci, 2023. **136**(12).
106. Shigeoka, T., et al., *On-Site Ribosome Remodeling by Locally Synthesized Ribosomal Proteins in Axons.* Cell Rep, 2019. **29**(11): p. 3605-3619 e10.
107. Baleriola, J. and U. Hengst, *Targeting axonal protein synthesis in neuroregeneration and degeneration.* Neurotherapeutics, 2015. **12**(1): p. 57-65.
108. Shigeoka, T., et al., *Dynamic Axonal Translation in Developing and Mature Visual Circuits.* Cell, 2016. **166**(1): p. 181-92.
109. Carter, D.A. and S.J. Lisney, *The numbers of unmyelinated and myelinated axons in normal and regenerated rat saphenous nerves.* J Neurol Sci, 1987. **80**(2-3): p. 163-71.
110. Gobrecht, P., et al., *Promotion of Functional Nerve Regeneration by Inhibition of Microtubule Detyrosination.* The Journal of Neuroscience, 2016. **36**(14): p. 3890-3902.
111. Li, D.D., et al., *Effects of delayed repair of peripheral nerve injury on the spatial distribution of motor endplates in target muscle.* Neural Regen Res, 2022. **17**(2): p. 459-464.

112. Gordon, T., R.B. Stein, and C.K. Thomas, *Organization of motor units following cross-reinnervation of antagonistic muscles in the cat hind limb.* J Physiol, 1986. **374**: p. 443-56.

113. Brushart, T.M., *Preferential reinnervation of motor nerves by regenerating motor axons.* J Neurosci, 1988. **8**(3): p. 1026-31.

114. Mira, J.C., *[Quantitative studies on the regeneration of myelinated nerve fibers. II. Variations of the number and size of regenerating nerve fibers after localized crushing or total section].* Arch Anat Microsc Morphol Exp, 1976. **65**(4): p. 255-84.

115. Fex Svennigsen, A. and L.B. Dahlin, *Repair of the Peripheral Nerve-Remyelination that Works.* Brain Sci, 2013. **3**(3): p. 1182-97.

116. Scalabrino, G., *Newly Identified Deficiencies in the Multiple Sclerosis Central Nervous System and Their Impact on the Remyelination Failure.* Biomedicines, 2022. **10**(4).

117. Podbielska, M., et al., *Myelin recovery in multiple sclerosis: the challenge of remyelination.* Brain Sci, 2013. **3**(3): p. 1282-324.

118. Costa-Mattioli, M. and P. Walter, *The integrated stress response: From mechanism to disease.* Science, 2020. **368**(6489).

119. Wek, R.C., H.Y. Jiang, and T.G. Anthony, *Coping with stress: eIF2 kinases and translational control.* Biochem Soc Trans, 2006. **34**(Pt 1): p. 7-11.

120. Wek, R.C., T.G. Anthony, and K.A. Staschke, *Surviving and Adapting to Stress: Translational Control and the Integrated Stress Response.* Antioxid Redox Signal, 2023. **39**(4-6): p. 351-373.

121. Wek, R.C., *Role of eIF2α Kinases in Translational Control and Adaptation to Cellular Stress.* Cold Spring Harb Perspect Biol, 2018. **10**(7).

122. Hinnebusch, A.G., *Translational regulation of GCN4 and the general amino acid control of yeast.* Annu Rev Microbiol, 2005. **59**: p. 407-50.

123. Lu, P.D., H.P. Harding, and D. Ron, *Translation reinitiation at alternative open reading frames regulates gene expression in an integrated stress response.* J Cell Biol, 2004. **167**(1): p. 27-33.

124. Vattem, K.M. and R.C. Wek, *Reinitiation involving upstream ORFs regulates ATF4 mRNA translation in mammalian cells.* Proc Natl Acad Sci U S A, 2004. **101**(31): p. 11269-74.

125. Novoa, I., et al., *Feedback inhibition of the unfolded protein response by GADD34-mediated dephosphorylation of eIF2alpha.* J Cell Biol, 2001. **153**(5): p. 1011-22.

126. De Miguel, C., et al., *Termination of the integrated stress response.* Science, 2026. **391**(6787): p. eadw5137.

127. Back, S.H., et al., *Translation attenuation through eIF2alpha phosphorylation prevents oxidative stress and maintains the differentiated state in beta cells.* Cell Metab, 2009. **10**(1): p. 13-26.

128. Scapin, C., et al., *Phosphorylation of eIF2α Promotes Schwann Cell Differentiation and Myelination in CMT1B Mice with Activated UPR.* J Neurosci, 2020. **40**(42): p. 8174-8187.

129. Cagnetta, R., et al., *Noncanonical Modulation of the eIF2 Pathway Controls an Increase in Local Translation during Neural Wiring.* Mol Cell, 2019. **73**(3): p. 474-489.e5.

130. Calcutt, N.A., et al., *Tactile allodynia and formalin hyperalgesia in streptozotocin-diabetic rats: effects of insulin, aldose reductase inhibition and lidocaine.* Pain, 1996. **68**(2-3): p. 293-9.
131. Chaplan, S.R., et al., *Quantitative assessment of tactile allodynia in the rat paw.* J Neurosci Methods, 1994. **53**(1): p. 55-63.
132. Fricker, L., et al., *A self-made, low-cost infrared system for evaluating the sciatic functional index in mice.* Neural Regen Res, 2016. **11**(5): p. 829-34.
133. Inserra, M.M., D.A. Bloch, and D.J. Terris, *Functional indices for sciatic, peroneal, and posterior tibial nerve lesions in the mouse.* Microsurgery, 1998. **18**(2): p. 119-24.
134. Maurel, P., et al., *Nectin-like proteins mediate axon Schwann cell interactions along the internode and are essential for myelination.* J Cell Biol, 2007. **178**(5): p. 861-74.
135. Asthana, P., et al., *Heat shock protein is a key therapeutic target for nerve repair in autoimmune peripheral neuropathy and severe peripheral nerve injury.* Brain Behav Immun, 2021. **91**: p. 48-64.
136. Di Paolo, A., et al., *Rat Sciatic Nerve Axoplasm Proteome Is Enriched with Ribosomal Proteins during Regeneration Processes.* J Proteome Res, 2021. **20**(5): p. 2506-2520.
137. Vergara, D., et al., *Proteomic expression profile of injured rat peripheral nerves revealed biological networks and processes associated with nerve regeneration.* J Cell Physiol, 2018. **233**(8): p. 6207-6223.
138. Shen, M., et al., *A proteome map of primary cultured rat Schwann cells.* Proteome Sci, 2012. **10**(1): p. 20.
139. Cifuentes-Diaz, C., et al., *Protein 4.1B contributes to the organization of peripheral myelinated axons.* PLoS One, 2011. **6**(9): p. e25043.
140. Patzig, J., et al., *Quantitative and integrative proteome analysis of peripheral nerve myelin identifies novel myelin proteins and candidate neuropathy loci.* J Neurosci, 2011. **31**(45): p. 16369-86.
141. Shi, G.D., et al., *iTRAQ-based proteomics profiling of Schwann cells before and after peripheral nerve injury.* Iran J Basic Med Sci, 2018. **21**(8): p. 832-841.
142. Calvo, M., et al., *Altered potassium channel distribution and composition in myelinated axons suppresses hyperexcitability following injury.* Elife, 2016. **5**: p. e12661.
143. Huang, Z.H., et al., *Inhibitor of DNA binding 2 accelerates nerve regeneration after sciatic nerve injury in mice.* Neural Regen Res, 2021. **16**(12): p. 2542-2548.
144. Zainul, Z., et al., *Collagen XIII Is Required for Neuromuscular Synapse Regeneration and Functional Recovery after Peripheral Nerve Injury.* J Neurosci, 2018. **38**(17): p. 4243-4258.
145. Altmann, C., et al., *Progranulin promotes peripheral nerve regeneration and reinnervation: role of notch signaling.* Mol Neurodegener, 2016. **11**(1): p. 69.
146. Lino, M.M., et al., *Mice lacking protease nexin-1 show delayed structural and functional recovery after sciatic nerve crush.* J Neurosci, 2007. **27**(14): p. 3677-85.
147. Bakooshli, M.A., et al., *Regeneration of neuromuscular synapses after acute and chronic denervation by inhibiting the gerozyme 15-prostaglandin dehydrogenase.* Sci Transl Med, 2023. **15**(717): p.

eadg1485.
148. Shen, C., et al., *Motoneuron Wnts regulate neuromuscular junction development.* Elife, 2018. **7**.
149. Je, H.S., et al., *Presynaptic protein synthesis required for NT-3-induced long-term synaptic modulation.* Mol Brain, 2011. **4**: p. 1.
150. Hwang, K.D., et al., *Restoring synaptic plasticity and memory in mouse models of Alzheimer's disease by PKR inhibition.* Mol Brain, 2017. **10**(1): p. 57.
151. Martinez, N.W., et al., *PKR-driven ISR signaling controls synaptic translation and structural plasticity in an age-dependent manner.* Neurobiol Dis, 2025: p. 107113.
152. Zhu, P.J., et al., *Suppression of PKR promotes network excitability and enhanced cognition by interferon-gamma-mediated disinhibition.* Cell, 2011. **147**(6): p. 1384-96.
153. Reimer, L., et al., *Inflammation kinase PKR phosphorylates alpha-synuclein and causes alpha-synuclein-dependent cell death.* Neurobiol Dis, 2018. **115**: p. 17-28.
154. Falcon, P., et al., *GCN2-Mediated eIF2alpha Phosphorylation Is Required for Central Nervous System Remyelination.* Int J Mol Sci, 2025. **26**(4).
155. Orsini, H., et al., *GCN2 kinase plays an important role triggering the remission phase of experimental autoimmune encephalomyelitis (EAE) in mice.* Brain Behav Immun, 2014. **37**: p. 177-86.
156. Pakos-Zebrucka, K., et al., *The integrated stress response.* EMBO Rep, 2016. **17**(10): p. 1374-1395.
157. Chen, C.W., et al., *Plasticity of the mammalian integrated stress response.* Nature, 2025. **641**(8065): p. 1319-1328.
158. Liu, B. and S.B. Qian, *Translational reprogramming in cellular stress response.* Wiley Interdiscip Rev RNA, 2014. **5**(3): p. 301-15.
159. Wang, H., et al., *Neurofilament proteins in axonal regeneration and neurodegenerative diseases.* Neural Regen Res, 2012. **7**(8): p. 620-6.
160. Lee, J.I., et al., *Functional recovery with histomorphometric analysis of nerves and muscles after combination treatment with erythropoietin and dexamethasone in acute peripheral nerve injury.* PLoS One, 2020. **15**(9): p. e0238208.
161. Dun, X.P. and D.B. Parkinson, *Visualizing peripheral nerve regeneration by whole mount staining.* PLoS One, 2015. **10**(3): p. e0119168.
162. Dubovy, P., et al., *A Conditioning Sciatic Nerve Lesion Triggers a Pro-regenerative State in Primary Sensory Neurons Also of Dorsal Root Ganglia Non-associated With the Damaged Nerve.* Front Cell Neurosci, 2019. **13**: p. 11.
163. Ouyang, Y., et al., *Single-cell transcriptomic landscape of sciatic nerve after transection injury.* J Neuroinflammation, 2025. **22**(1): p. 205.
164. Kwon, Y.K., et al., *Activation of ErbB2 during wallerian degeneration of sciatic nerve.* J Neurosci, 1997. **17**(21): p. 8293-9.
165. Gong, L., et al., *Genetic changes in rat proximal nerve stumps after sciatic nerve transection.* Ann Transl Med, 2019. **7**(23): p. 763.

166. Guertin, A.D., et al., *Microanatomy of axon/glial signaling during Wallerian degeneration.* J Neurosci, 2005. **25**(13): p. 3478-87.
167. Chen, B., et al., *Analysis of Schwann Cell Migration and Axon Regeneration Following Nerve Injury in the Sciatic Nerve Bridge.* Front Mol Neurosci, 2019. **12**: p. 308.
168. Li, L., et al., *Ascorbic Acid Facilitates Neural Regeneration After Sciatic Nerve Crush Injury.* Front Cell Neurosci, 2019. **13**: p. 108.
169. Kirsch, M., et al., *Wallerian degeneration and axonal regeneration after sciatic nerve crush are altered in ICAM-1-deficient mice.* Cell Tissue Res, 2009. **338**(1): p. 19-28.
170. Gaudet, A.D., P.G. Popovich, and M.S. Ramer, *Wallerian degeneration: gaining perspective on inflammatory events after peripheral nerve injury.* J Neuroinflammation, 2011. **8**: p. 110.
171. Nadeau, S., et al., *Functional recovery after peripheral nerve injury is dependent on the pro-inflammatory cytokines IL-1beta and TNF: implications for neuropathic pain.* J Neurosci, 2011. **31**(35): p. 12533-42.
172. Tachiya, D., T. Sato, and H. Ichikawa, *Nerve Injury Increases the Expression of Alpha-2/Delta-1 Subunit of L-Type Calcium Channel in Sensory Neurons of Rat Spinal and Trigeminal Nerves.* Ann Neurosci, 2018. **24**(4): p. 191-200.
173. Jeub, M., et al., *Partial sciatic nerve ligation leads to an upregulation of Ni(2+)-resistant T-type Ca(2+) currents in capsaicin-responsive nociceptive dorsal root ganglion neurons.* J Pain Res, 2019. **12**: p. 635-647.
174. Schafers, M., et al., *Tumor necrosis factor-alpha (TNF) regulates the expression of ICAM-1 predominantly through TNF receptor 1 after chronic constriction injury of mouse sciatic nerve.* Acta Neuropathol, 2002. **104**(2): p. 197-205.
175. Schafers, M., et al., *Selective increase of tumour necrosis factor-alpha in injured and spared myelinated primary afferents after chronic constrictive injury of rat sciatic nerve.* Eur J Neurosci, 2003. **17**(4): p. 791-804.
176. George, A., A. Buehl, and C. Sommer, *Tumor necrosis factor receptor 1 and 2 proteins are differentially regulated during Wallerian degeneration of mouse sciatic nerve.* Exp Neurol, 2005. **192**(1): p. 163-6.
177. Sacerdote, P., et al., *Transient early expression of TNF-alpha in sciatic nerve and dorsal root ganglia in a mouse model of painful peripheral neuropathy.* Neurosci Lett, 2008. **436**(2): p. 210-3.
178. Wang, Y., et al., *Pathogenic TNF-alpha drives peripheral nerve inflammation in an Aire-deficient model of autoimmunity.* Proc Natl Acad Sci U S A, 2022. **119**(4).
179. Tanaka, K. and H.D. Webster, *Myelinated fiber regeneration after crush injury is retarded in sciatic nerves of aging mice.* J Comp Neurol, 1991. **308**(2): p. 180-7.
180. Zhang, L., D. Johnson, and J.A. Johnson, *Deletion of Nrf2 impairs functional recovery, reduces clearance of myelin debris and decreases axonal remyelination after peripheral nerve injury.* Neurobiol Dis, 2013. **54**: p. 329-38.

181. da Silva, T.F., et al., *Peripheral nervous system plasmalogens regulate Schwann cell differentiation and myelination.* J Clin Invest, 2014. **124**(6): p. 2560-70.
182. Makoukji, J., et al., *Lithium enhances remyelination of peripheral nerves.* Proc Natl Acad Sci U S A, 2012. **109**(10): p. 3973-8.
183. Kim, H.W., et al., *Long-term tactile hypersensitivity after nerve crush injury in mice is characterized by the persistence of intact sensory axons.* Pain, 2023. **164**(10): p. 2327-2342.
184. Hossain-Ibrahim, M.K., et al., *Analysis of axonal regeneration in the central and peripheral nervous systems of the NG2-deficient mouse.* BMC Neurosci, 2007. **8**: p. 80.
185. Stettner, M., et al., *The Role of Peripheral Myelin Protein 2 in Remyelination.* Cell Mol Neurobiol, 2018. **38**(2): p. 487-496.
186. Zhou, Y. and L. Notterpek, *Promoting peripheral myelin repair.* Exp Neurol, 2016. **283**(Pt B): p. 573-80.
187. Tong, L.L., et al., *Differential motor and sensory functional recovery in male but not female adult rats is associated with remyelination rather than axon regeneration after sciatic nerve crush.* Neuroreport, 2015. **26**(7): p. 429-37.
188. Duman, M., et al., *Theophylline Induces Remyelination and Functional Recovery in a Mouse Model of Peripheral Neuropathy.* Biomedicines, 2022. **10**(6).
189. Morrison, B.M., et al., *Deficiency in monocarboxylate transporter 1 (MCT1) in mice delays regeneration of peripheral nerves following sciatic nerve crush.* Exp Neurol, 2015. **263**: p. 325-38.
190. Pavic, R., et al., *Side distinct sciatic nerve recovery differences between rats and mice.* Somatosens Mot Res, 2008. **25**(3): p. 163-70.
191. Xiong, Y., et al., *Peripheral Neuropathy and Hindlimb Paralysis in a Mouse Model of Adipocyte-Specific Knockout of Lkb1.* EBioMedicine, 2017. **24**: p. 127-136.
192. Cahill, L.S., et al., *Aged hind-limb clasping experimental autoimmune encephalomyelitis models aspects of the neurodegenerative process seen in multiple sclerosis.* Proc Natl Acad Sci U S A, 2019. **116**(45): p. 22710-22720.
193. Kang, M.S., et al., *Neuroprotective Effect of Nypa fruticans Wurmb by Suppressing TRPV1 Following Sciatic Nerve Crush Injury in a Rat.* Nutrients, 2020. **12**(9).
194. Ruan, Y., et al., *An effective and concise device for detecting cold allodynia in mice.* Sci Rep, 2018. **8**(1): p. 14002.
195. Freria, C.M., et al., *Impairment of toll-like receptors 2 and 4 leads to compensatory mechanisms after sciatic nerve axotomy.* J Neuroinflammation, 2016. **13**(1): p. 118.
196. Chen, Y.S., S.S. Chung, and S.K. Chung, *Aldose reductase deficiency improves Wallerian degeneration and nerve regeneration in diabetic thy1-YFP mice.* J Neuropathol Exp Neurol, 2010. **69**(3): p. 294-305.
197. Berg, A., et al., *Axonal regeneration after sciatic nerve lesion is delayed but complete in GFAP- and vimentin-deficient mice.* PLoS One, 2013. **8**(11): p. e79395.
198. Zhang, K., M. Jiang, and Y. Fang, *The Drama of Wallerian Degeneration: The Cast, Crew, and Script.* Annu Rev Genet, 2021. **55**: p. 93-113.

199. Tian, X., et al., *Targeting the Integrated Stress Response in Cancer Therapy.* Front Pharmacol, 2021. **12**: p. 747837.
200. Licari, E., L. Sánchez-Del-Campo, and P. Falletta, *The two faces of the Integrated Stress Response in cancer progression and therapeutic strategies.* Int J Biochem Cell Biol, 2021. **139**: p. 106059.
201. Jang, S.Y., et al., *Schwann cell dedifferentiation-associated demyelination leads to exocytotic myelin clearance in inflammatory segmental demyelination.* Glia, 2017. **65**(11): p. 1848-1862.
202. Wong, K.M., E. Babetto, and B. Beirowski, *Axon degeneration: make the Schwann cell great again.* Neural Regen Res, 2017. **12**(4): p. 518-524.
203. Stoll, G. and H.W. Müller, *Nerve injury, axonal degeneration and neural regeneration: basic insights.* Brain Pathol, 1999. **9**(2): p. 313-25.
204. Martínez, N.W., et al., *PKR-driven ISR signaling controls synaptic translation and structural plasticity in an age-dependent manner.* Neurobiol Dis, 2025. **216**: p. 107113.
205. Sidoli, M., et al., *Ablation of Perk in Schwann Cells Improves Myelination in the S63del Charcot-Marie-Tooth 1B Mouse.* J Neurosci, 2016. **36**(44): p. 11350-11361.
206. Khoutorsky, A., et al., *eIF2alpha phosphorylation controls thermal nociception.* Proc Natl Acad Sci U S A, 2016. **113**(42): p. 11949-11954.
207. Li, Q., et al., *Hippocampal PKR/NLRP1 Inflammasome Pathway Is Required for the Depression-Like Behaviors in Rats with Neuropathic Pain.* Neuroscience, 2019. **412**: p. 16-28.
208. Zhang, J., et al., *Activation of Double-Stranded RNA-Activated Protein Kinase in the Dorsal Root Ganglia and Spinal Dorsal Horn Regulates Neuropathic Pain Following Peripheral Nerve Injury in Rats.* Neurotherapeutics, 2022. **19**(4): p. 1381-1400.
209. Khoutorsky, A., et al., *eIF2α phosphorylation controls thermal nociception.* Proc Natl Acad Sci U S A, 2016. **113**(42): p. 11949-11954.
210. Twiss, J.L. and C.N. Buchanan, *Regulation of Subcellular Protein Synthesis for Restoring Neural Connectivity.* Int J Mol Sci, 2025. **26**(15).
211. Perry, G.W. and D.L. Wilson, *Protein synthesis and axonal transport during nerve regeneration.* J Neurochem, 1981. **37**(5): p. 1203-17.
212. Twiss, J.L., et al., *Intra-axonal protein synthesis - a new target for neural repair?* Neural Regen Res, 2016. **11**(9): p. 1365-1367.
213. Zheng, J.Q., et al., *A functional role for intra-axonal protein synthesis during axonal regeneration from adult sensory neurons.* J Neurosci, 2001. **21**(23): p. 9291-303.
214. Taveggia, C., M.L. Feltri, and L. Wrabetz, *Signals to promote myelin formation and repair.* Nat Rev Neurol, 2010. **6**(5): p. 276-87.
215. Xiao, Y., et al., *High-resolution live imaging reveals axon-glia interactions during peripheral nerve injury and repair in zebrafish.* Dis Model Mech, 2015. **8**(6): p. 553-64.
216. Glenn, T.D. and W.S. Talbot, *Signals regulating myelination in peripheral nerves and the Schwann cell response to injury.* Curr Opin Neurobiol, 2013. **23**(6): p. 1041-8.

217. White, R. and E.M. Krämer-Albers, *Axon-glia interaction and membrane traffic in myelin formation.* Front Cell Neurosci, 2014. **7**: p. 284.
218. Fricker, F.R., et al., *Axonally derived neuregulin-1 is required for remyelination and regeneration after nerve injury in adulthood.* J Neurosci, 2011. **31**(9): p. 3225-33.
219. Fledrich, R., et al., *Axo-glial interdependence in peripheral nerve development.* Development, 2019. **146**(21).
220. Painter, M.W., et al., *Diminished Schwann cell repair responses underlie age-associated impaired axonal regeneration.* Neuron, 2014. **83**(2): p. 331-343.
221. Yang, D.P., et al., *Schwann cell proliferation during Wallerian degeneration is not necessary for regeneration and remyelination of the peripheral nerves: axon-dependent removal of newly generated Schwann cells by apoptosis.* Mol Cell Neurosci, 2008. **38**(1): p. 80-8.

Figures

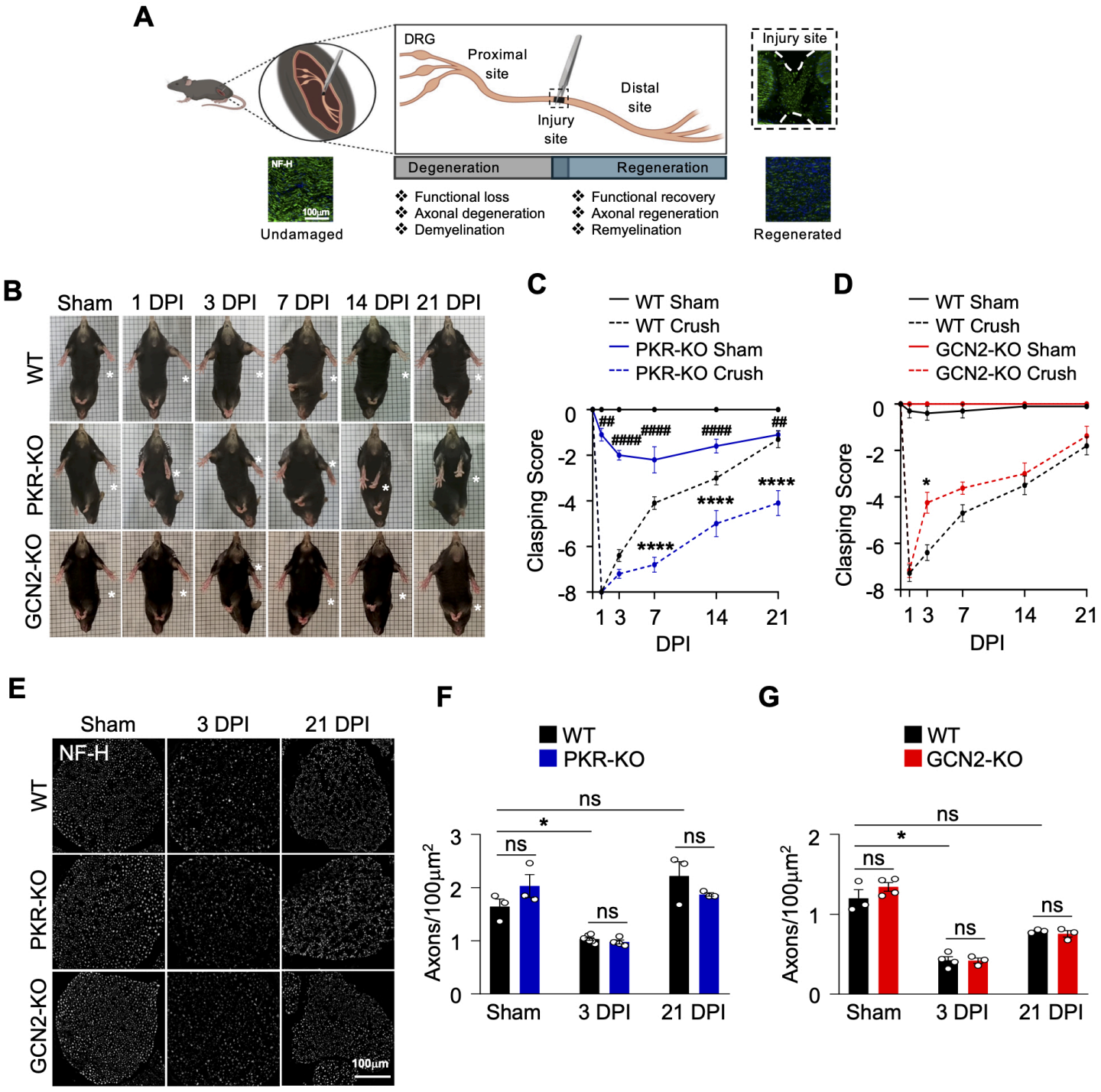


Figure 1

PKR deficiency modulates axonal density and sensorimotor functional loss and recovery following sciatic nerve crush injury. (A) Schematic representation of the experimental design and the sciatic nerve regions analyzed. Mice were subjected to sciatic nerve crush injury. The schematic illustrates the main events occurring after injury during the degenerative and regenerative processes. Representative immunofluorescence images of neurofilament heavy chain (NF-H, green) depict the organization of the sciatic nerve under uninjured, injured (injury site), and regenerated conditions; nuclei are counterstained with DAPI (blue). Scale bar: 100 µm. (B) Representative images of the right hindlimbs showing the limb

angle and digit extension (white asterisk) at 1, 3, 7, 14, and 21 days post-injury (DPI) or after sham surgery (no asterisk) in WT, PKR-KO, or GCN2-KO mice. Quantification and comparison of crushed and contralateral sham hindlimbs of (C) WT (n = 10) and PKR-KO (n = 10) mice and (D) WT (n = 10) and GCN2-KO mice (n = 8). Data are presented as mean ± SEM. Two-tailed Mann–Whitney test; for crushed, *p < 0.05, ****p < 0.0001; for sham, ##p < 0.01, ####p < 0.0001. Only significant differences are indicated. (E) Representative confocal images (40×) of sciatic nerves from WT, PKR-KO, and GCN2-KO mice stained for the axonal marker neurofilament heavy chain (NF-H) at 3 and 21 DPI or under sham conditions. Scale bar: 100 μm. Axonal density was quantified by counting binarized NF-H-positive particles in confocal images, as illustrated in (E). (F) Quantification of axonal density (axons/100 μm²) in WT and PKR-KO sciatic nerves at 3 and 21 DPI or under sham conditions. (G) Quantification of axonal density (axons/100 μm²) in WT and GCN2-KO sciatic nerves at 3 and 21 DPI or under sham conditions. Two-tailed Mann–Whitney test; ns, non-significant; *p < 0.05.

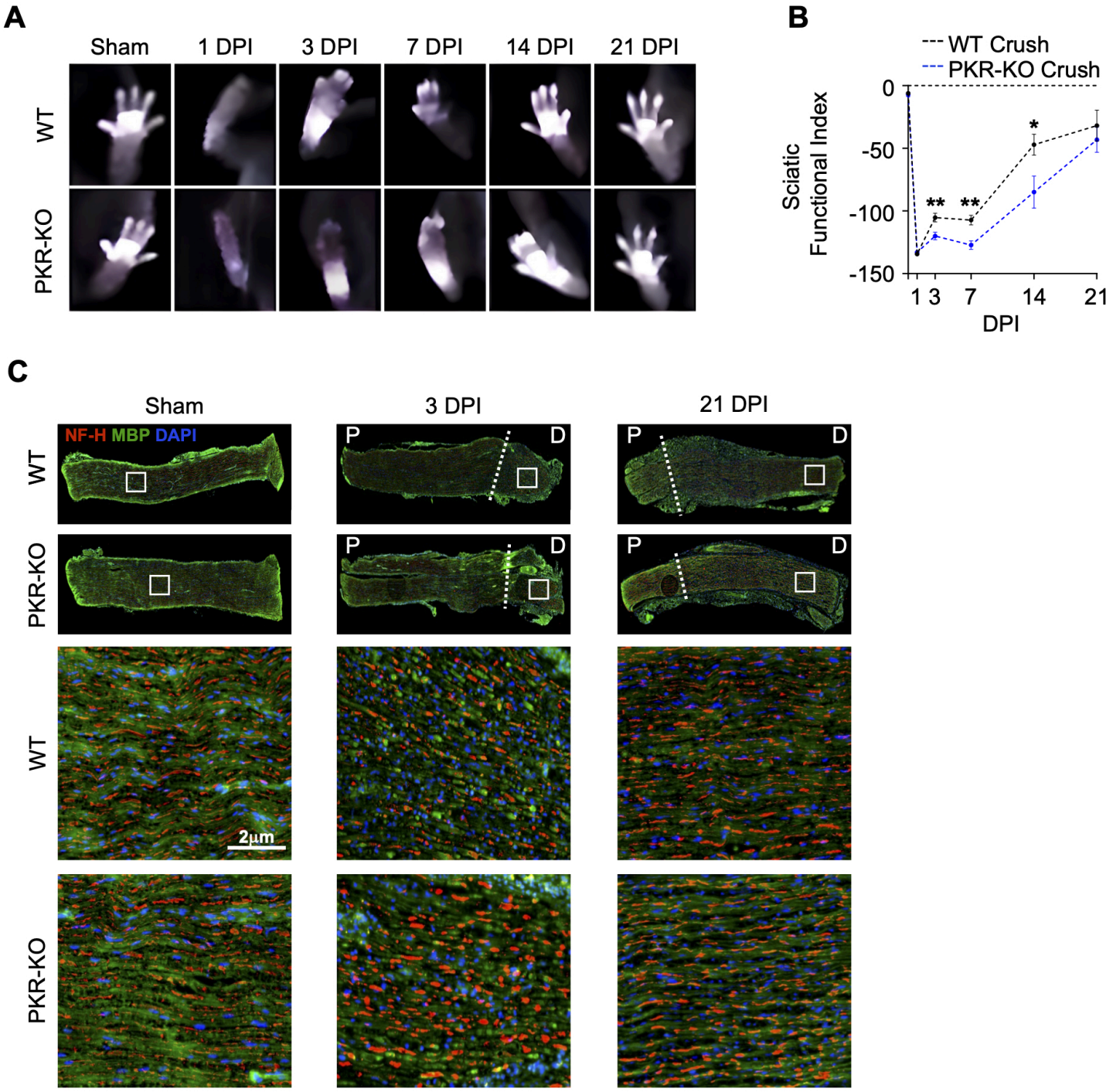


Figure 2

PKR deficiency affects sciatic nerve functional recovery without altering axonal organization following sciatic nerve crush injury. (A) Representative hindlimb digital footprints at 1, 3, 7, 14, and 21 days post-injury (DPI) or under sham conditions in WT and PKR-KO mice. (B) Quantification of the Sciatic Functional Index (SFI) of crushed and contralateral sham hindlimbs in WT (n = 10) and PKR-KO (n = 10) mice. Data are presented as mean ± SEM. Two-tailed Mann–Whitney test; *p < 0.05, **p < 0.01. Only significant differences are indicated. (C) Representative immunofluorescence images of longitudinal sections of sciatic nerves from WT and PKR-KO mice under sham conditions and at 3 and 21 DPI

following sciatic nerve crush injury. Whole-nerve views illustrate overall nerve morphology, with dashed boxes indicating the regions shown at higher magnification below; dashed lines indicate the injury site. Letters P and D denote proximal and distal nerve regions relative to the crush site, respectively. High-magnification images show axons labeled with neurofilament heavy chain (NF-H, red), myelin basic protein (MBP, green), and nuclei counterstained with DAPI (blue). Scale bar: 2 μm.

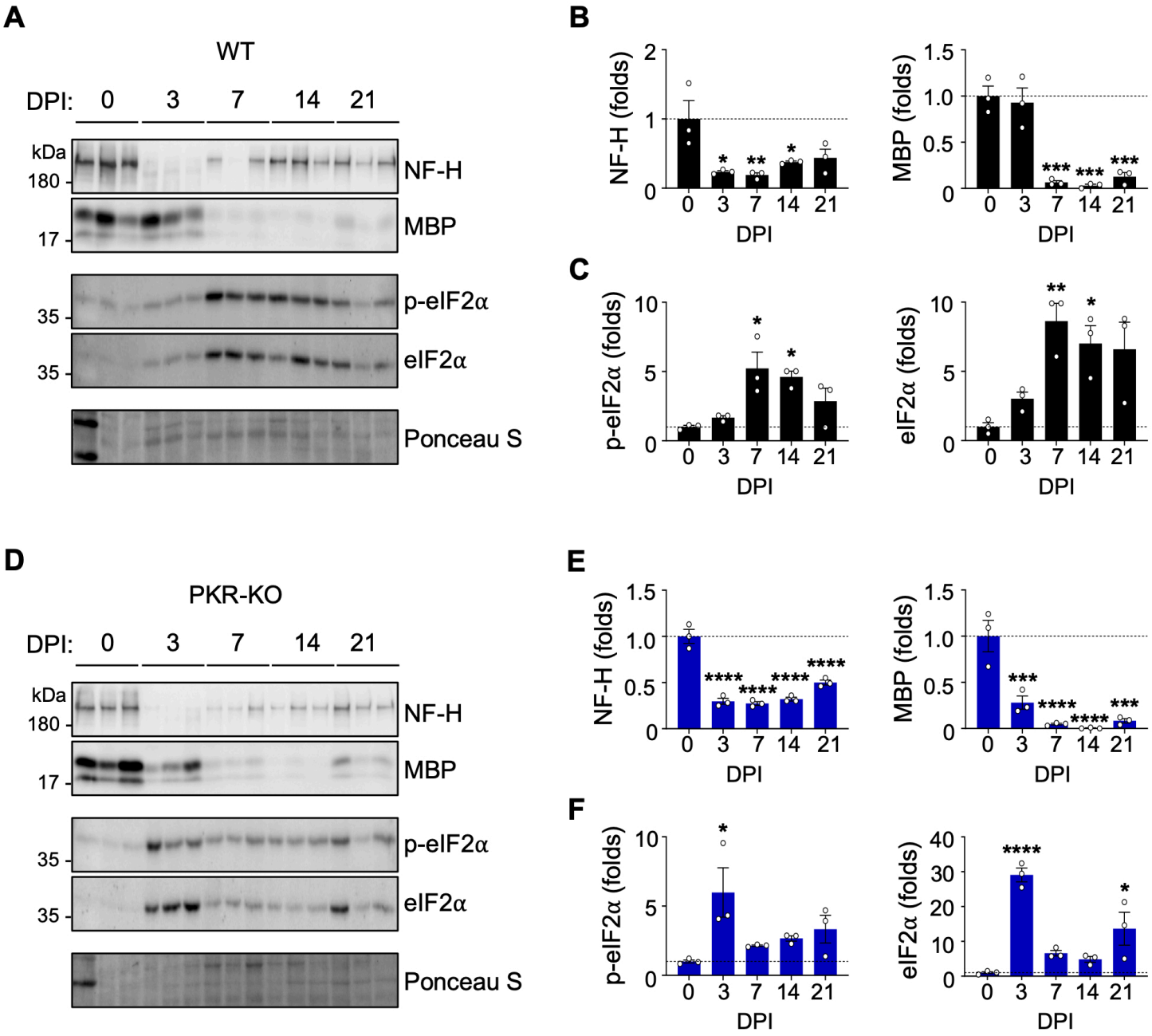


Figure 3

Dynamics of eIF2a phosphorylation and nerve structural integrity following sciatic nerve injury in WT and PKR-KO mice. (A) Western blot analysis showing detection of NF-H, MBP, eIF2a, and phosphorylated eIF2a (p-eIF2a) in sciatic nerve lysates from WT mice. Each lane represents the sciatic nerve from a single animal; 12 μg of total protein were loaded per lane. Protein levels were quantified by band intensity and normalized to total protein levels (Ponceau S). Quantification of NF-H and MBP protein

levels (B) and of phosphorylated eIF2α (p-eIF2a) and total eIF2a levels (C). (D) Same Western blot analysis in sciatic nerve lysates from PKR-KO mice. Panels (E) and (F) show the quantification of NF-H and MBP protein levels and of phosphorylated eIF2a (p-eIF2a) and total eIF2a levels, respectively, from PKR-KO mice. Data are presented as fold change relative to day 0. Bars represent mean ± SEM from three mice per time point (n = 3). Statistical analysis was performed using one-way ANOVA followed by Tukey's multiple comparison test; *p < 0.05, **p < 0.01, ***p < 0.001, ****p < 0.0001. Only significant differences are indicated.

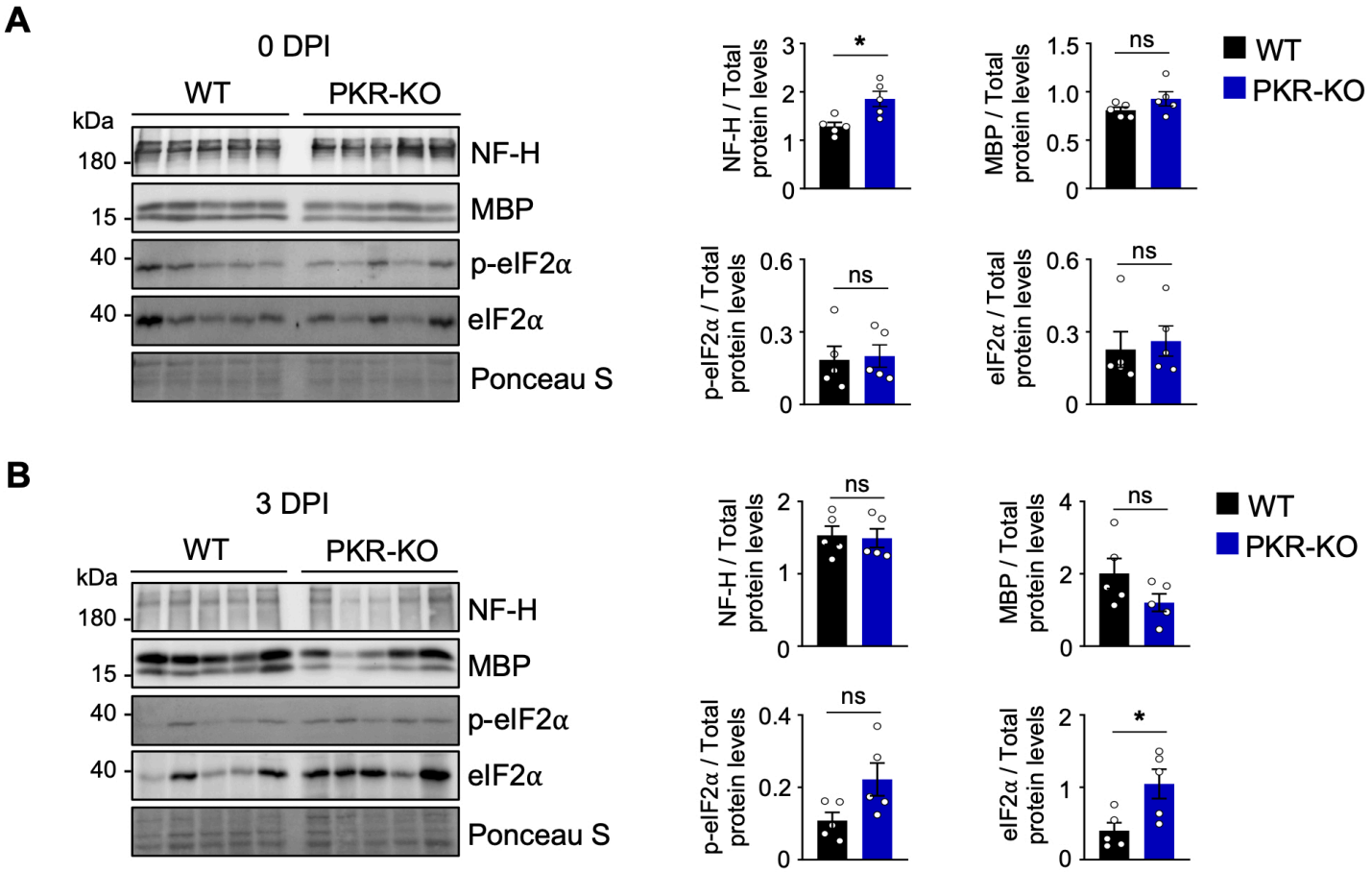


Figure 4

Comparative analysis of ISR activation in WT and PKR-KO mice during loss of sciatic nerve integrity and structure. Western blot analysis and quantification of neurofilament heavy chain (NF-H), myelin basic protein (MBP), total eIF2α, and phosphorylated eIF2a (p-eIF2a) in sciatic nerve lysates from wild-type (WT) and PKR-KO mice at 0 (A) and 3 (B) days post-injury (DPI). Ponceau S staining was used as a loading control. Each lane corresponds to one animal; 12 µg of total protein were loaded per lane. Data are presented as mean ± SEM (n = 5 per group). Statistical analysis was performed using a two-tailed Welch's t-test: ns, non-significant; *p < 0.05.

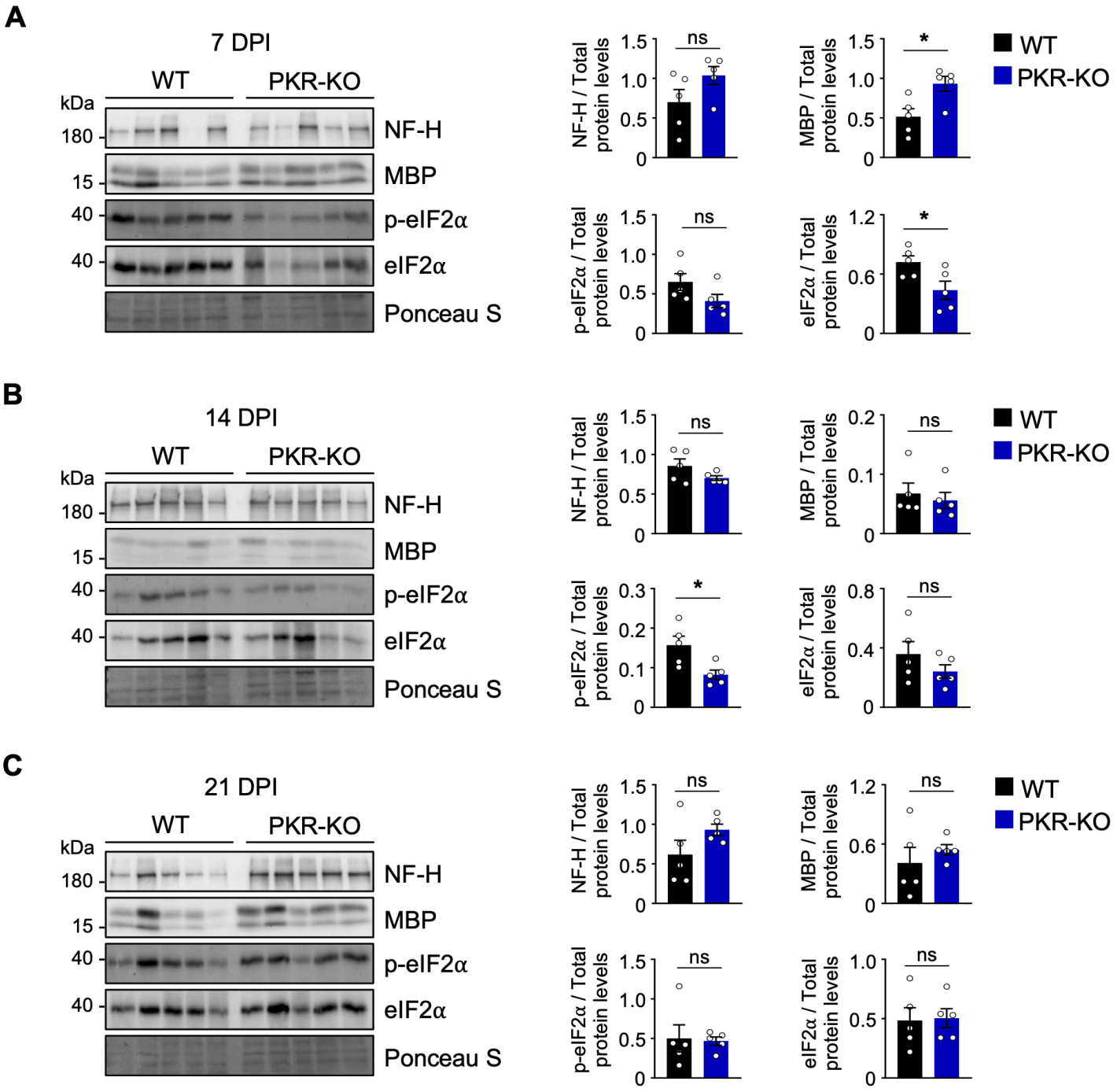


Figure 5

Comparative analysis of ISR activation in WT and PKR-KO mice during recovery of sciatic nerve integrity and structure. Western blot analysis and quantification of neurofilament heavy chain (NF-H), myelin basic protein (MBP), total eIF2α, and phosphorylated eIF2a (p-eIF2a) in sciatic nerve lysates from wild-type (WT) and PKR-KO mice at 7 (A), 14 (B), and 21 (C) days post-injury (DPI). Ponceau S staining was used as a loading control. Each lane corresponds to one animal; 12 µg of total protein were loaded per lane. Data are presented as mean ± SEM (n = 5 per group). Statistical analysis was performed using a two-tailed Welch's t-test: ns, non-significant; *p < 0.05.

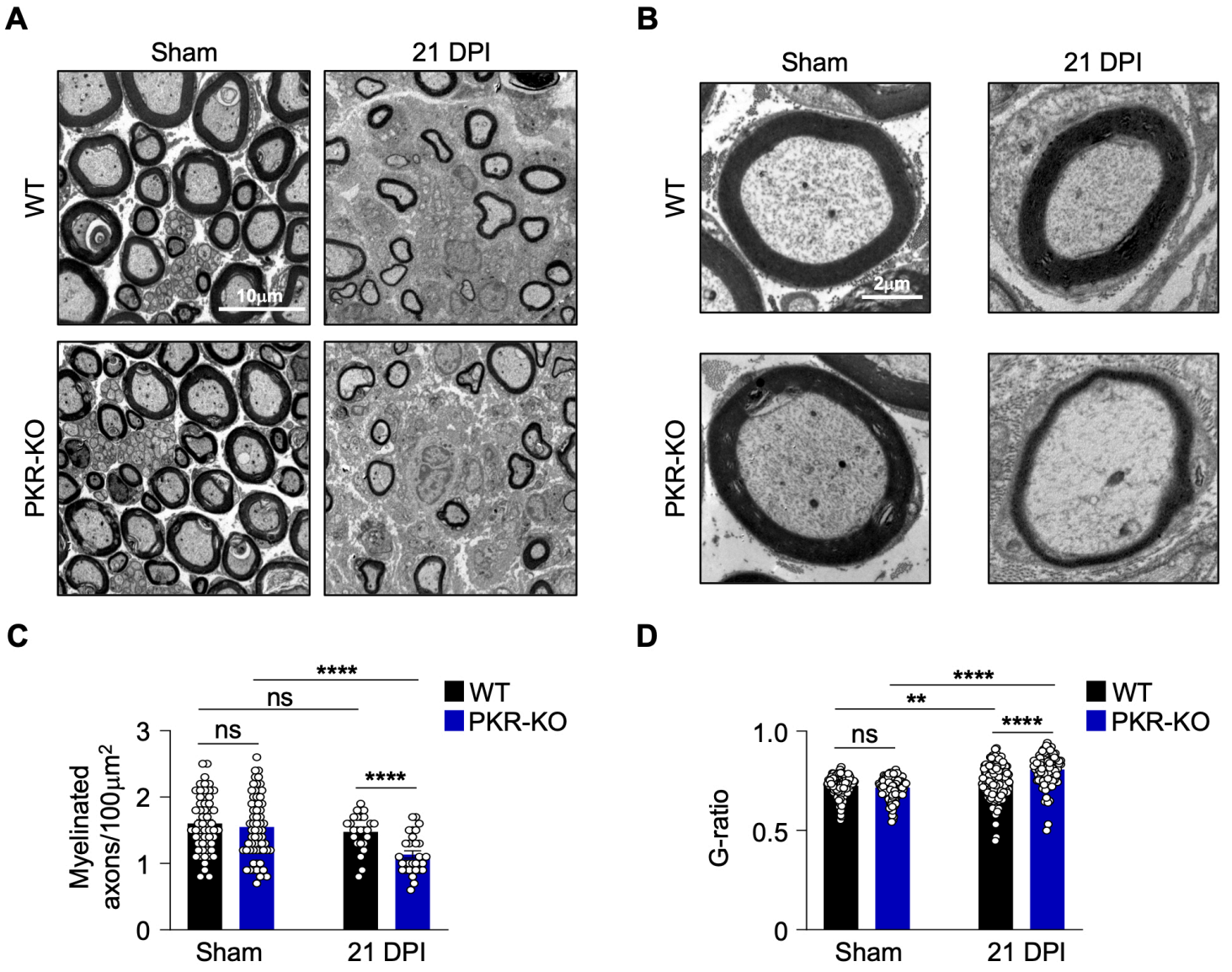


Figure 6

Ultrastructure of myelinated axons after sciatic nerve injury in the absence of PKR. (A) Representative transmission electron microscopy images of cross-sections of the distal region of the sciatic nerve in wild-type (WT) and PKR-KO mice under sham (uninjured) conditions and at 21 days post-injury (DPI). Scale bar: 10 µm. (B) Higher-magnification transmission electron microscopy images of representative myelinated axons from the distal region of the sciatic nerve in WT and PKR-KO mice under sham conditions and at 21 DPI, illustrating axonal caliber and myelin sheath morphology. Scale bar: 2 µm. (C) Quantification of myelinated axon density (myelinated axons/100 µm²) in WT and PKR-KO sciatic nerves under sham and 21 DPI conditions. (D) g-ratio analysis (axon diameter/fiber diameter) in WT and PKR-KO sciatic nerves under sham and 21 DPI conditions. Data are presented as mean ± SEM (n = 3 per group). Statistical analysis was performed using Welch's t-test: ns, non-significant; **p < 0.01, ****p < 0.0001.

Supplementary Files

This is a list of supplementary files associated with this preprint. Click to download.

- SUPPLEMENTARYFIGURE1MartinezMorales2026.jpg
- SUPPLEMENTARYFIGURE2MartinezMorales2026.jpg
- SUPPLEMENTARYFIGURE3MartinezMorales2026.jpg
- SUPPLEMENTARYFIGURE4MartinezMorales2026.jpg
- SUPPLEMENTARYFIGURE5MartinezMorales2026.jpg
- SUPPLEMENTARYFIGURE6MartinezMorales2026.jpg
- SUPPLEMENTARYFIGURE7.Fulllengthwesternblotmembranes.pdf
- SUPPLEMENTARYFIGURELEGENDS.docx